Deterioration effects of wet environments and brown rot fungus *Coniophora puteana* on pine wood in the archaeological site of Biskupin (Poland)

Jeannette Jacqueline Łucejko[1], Marco Mattonai[1], Magdalena Zborowska[2], Diego Tamburini[3], Grzegorz Cofta[2], Emma Cantisani[4], Jozef Kúdela[5], Caroline Cartwright[3], Maria Perla Colombini[1,4], Erika Ribechini[1,4], Francesca Modugno[1.4]

[1]Department of Chemistry and Industrial Chemistry University of Pisa, 56124 PI, Italy
[2]Institute of Chemical Wood Technology, Poznań University of Life Sciences, 60-627 Poznań, Poland
[3]Department of Scientific Research, The British Museum, WC1B 3DG, London, United Kingdom
[4]Institute for the Conservation and Valorization of Cultural Heritage, CNR, 50019 Sesto Fiorentino (FI), Italy
[5]Department of Wood Science, Technical University in Zvolen, SK-96053 Zvolen, Slovak Republic

Abstract

The archaeological site of Biskupin (Poland) is a prehistoric settlement dating to the 8th century BC, situated on a marshy island. Excavations started in 1934 and a considerable number of wooden artifacts was found in the lake water. Unfortunately, during many years of archaeological excavations, wooden remains deposited in the trenches were exposed to degradation and underwent considerable decomposition. Among the main causes of wood degradation, fungi and bacteria were the most destructive ones.

The chemical effects induced by fungi and bacteria on wood are not well known or studied. Here we present the investigation of a set of pine wood samples (*Pinus sylvestris*) buried in the Biskupin site, with the aim of reproducing the burial conditions of the original archaeological wood. Two monitoring stations (wet peat and lake water) were chosen and the samples were then removed from these burial environments after four and ten years. After removal, the samples were exposed to laboratory-controlled attack by the brown rot fungus *Coniophora puteana*. The final aim was to evaluate the effects of fungal activity on the wood substrates with different degrees of natural degradation. The study is part of an experiment designed to evaluate the short-term effects of the *in situ* preservation strategy adopted for the Biskupin archaeological woods.

Various techniques were used to assess the physical and chemical degradation of the wood. The morphological changes induced by the exposure to the burial environment and by the action of the fungi were investigated using scanning electron microscopy (SEM). The chemical state of the wood was evaluated by using infrared spectroscopy (FTIR), analytical pyrolysis coupled with gas chromatography and mass spectrometry (Py-GC-MS) and XRD spectroscopy.

Fungal action caused the depletion of polysaccharides resulting in mass loss and the FTIR spectra of the wood samples highlighted that cellulose was more degraded with respect to hemicelluloses. This trend correlated with an increase in the relative abundance of furans, which are among the main pyrolysis products of polysaccharides. Fungal attack also

induced oxidation of lignin and an increase in the crystallinity index of cellulose, which points towards a preferential metabolisation of amorphous cellulose. The overall results highlighted that the burial in these wet environments caused changes mostly in the hemicelluloses, whereas the fungal attack was mainly directed to cellulose degradation.

Keywords

Wood degradation, brown rot fungi, archaeological waterlogged wood, SEM, FTIR, XRD, Py-GC-MS

1. Introduction

The archaeological site of Biskupin (Poland) is a prehistoric settlement discovered in 1933, which dateto the Bronze and early Iron Ages (8th century BC). The settlement was situated on a marshy island and several excavation campaigns were conducted between 1934 and 1974 in an area of about 2 ha. [1]. Considerable quantities of wooden artifacts were found in the lake water. The fortified settlement, surrounded by a wooden breakwater, consisted of around one hundred houses. Buildings and streets were made of wood. During the archaeological excavations, wooden remains deposited in the trenches were exposed to degradation and underwent decomposition, due mainly to the action of microorganisms such as fungi and bacteria. In the 1970s, an attempt was made to preserve the excavated wood with phenol resin, leading to considerable damage of the treated archaeological wood [1]. Despite the promising results with consolidating agents showed by recent publications, no additional preservation strategies were adopted [2-6].

After this attempt, it was decided to adopt an *in situ* conservation strategy by leaving the wood remains in the environment in which they had been found, either in the wet peaty ground or in water. At Biskupin today it is possible to visit a reconstruction of the ancient village (Figure 1), but the archaeological wood has been reburied and is kept underground.

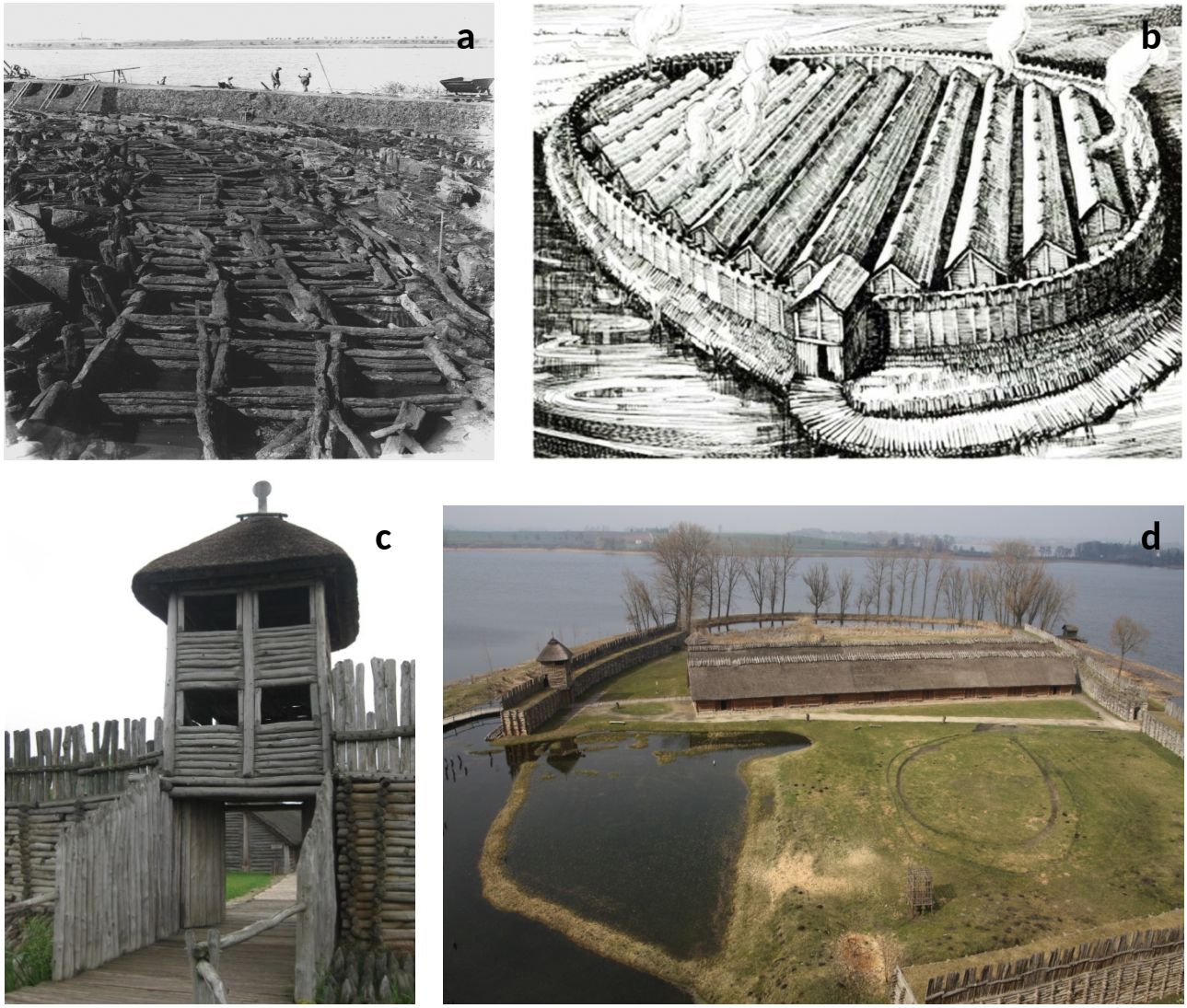

Figure 1. **a)** Photograph taken at Biskupin during the excavations before 1936 showing the archaeological wood remains [7]; **b)** a reconstruction drawing of the Bronze Age village (Biskupin Museum Archives); **c, d)** Biskupin archaeological site as it appears today: some of the structures of the village have been reconstructed with new wood, but the original archaeological wood is preserved *in situ* underground or underwater.

The action of fungi and bacteria [8] represents a significant risk for the preservation and display of waterlogged archaeological wooden artifacts. In fact, although the action of fungi is limited or absent in waterlogged anaerobic environments, archaeological wood is prone to severe attack by fungi when removed from the burial environment, as testified by a considerable amount of the Biskupin material. Biocide agents should always be introduced in archaeological wood material as part of *in situ* preservation strategy.

The effects of fungi and bacteria on wood are an important research field in wood chemistry [9-14]. Different spectroscopic techniques (FTIR, FT-Raman and NMR), thermochemical methods (TGA, Py-MS and Py-GC-MS) and wet chemical methods have been developed and applied to measure the extent of wood deterioration induced by brown rot fungi [15-25]. Data reported in the literature indicate that brown rot fungi mainly

attack hemicelluloses and cellulose, causing their depolymerisation and leaving a fragile wood, rich in lignin. In addition, two-dimensional solution-state nuclear magnetic resonance spectroscopy (2D-NMR) revealed that some brown rot fungi can also promote lignin demethylation and oxidation [15, 16]. Using ^{13}C-labeled tetramethylammonium hydroxide thermochemolysis (^{13}C-TMAH) and solid state ^{13}C NMR, Filley *et al.* [17] demonstrated a positive correlation between lignin demethylation and polysaccharide loss in spruce sapwood inoculated with brown rot fungi, suggesting that lignin demethylation may play a mechanistic role in polysaccharide depletion.
Interesting results have recently been obtained by XRD on poplar wood after brown rot decay, showing that fungal decay only changes the crystallinity of cellulose and has no influence on the structure of the unit cells. During the 12-week decay process, the degree of crystallinity increased, which can be explained by the preferred initial removal of the paracrystalline part of cellulose [26]. Slightly different data, including an increase in crystallinity early in the decay process followed by a decrease, have previously been observed by other researchers examining wood decayed by brown rot fungi [27]. The phenomenon has been attributed to the initial removal of hemicelluloses and other amorphous materials, followed by a fungal attack on the crystalline cellulose.

The drying process of waterlogged archaeological wood is another risk that adds to the biological threats, as it can cause irreversible mechanical damage and shrinkage. No satisfactory strategy is available for the preservation of archaeological wood once it has been dried, although polyethylene glycol (PEG) is probably the method that has been adopted most [28, 29]. For this reason, at present, *in situ* preservation of large wet wooden objects in marine or lake environments and in wet soil is proposed as an preferential choice by many wood preservation experts in Europe [1, 30, 31].

The results of the chemical investigation of archaeological wood from the Biskupin site were recently described [31-34], showing that a significant carbohydrate fraction is still present in the wood, even though polysaccharides are usually more susceptible to degradation than lignin in waterlogged environments [32]. For this reason, there is an urgent need for additional information on how to preserve from further degradation the holocellulose fraction in these samples. In this work, we describe the investigation of a set of pine wood samples (*Pinus sylvestris*) buried in the Biskupin site in two different monitoring stations (lake water and peat), in order to reproduce the burial conditions of the archaeological wood. Samples of the wood material were analysed after 4 and 10 years of burial in the two monitoring stations, as a part of a wider experiment designed to evaluate the short-term effects of the *in situ* preservation strategy adopted for the Biskupin archaeological woods [35]. After removal from the burial environments, the pine wood samples were exposed to laboratory-controlled attack by the brown rot fungus *Coniophora puteana* (Schumacher ex Fries) Karstein BAM Ebw. The aim was to evaluate the effects of fungal activity on the carbohydrate fraction of wood substrates after natural degradation.

Various techniques were used to assess the physical and chemical state of the wood samples, selected in order to be as informative as possible for the evaluation of wood alteration [36]. Physical properties such as moisture content and conventional density were determined because they are the most commonly-used parameters to establish the

mechanical stability of degraded wood [31]. Following an established successful approach [34, 37], the morphological changes induced by the exposure to the burial environment and by the fungal action were studied by examining the transverse, radial longitudinal and tangential longitudinal sections of the wood samples by scanning electron microscopy (SEM). The chemical state of preservation was evaluated by infrared spectroscopy (FTIR) and analytical pyrolysis coupled with gas chromatography and mass spectrometry (Py-GC-MS). FTIR analyses of the chemical changes occurring in pine wood decayed by *C. puteana* focused on the relative changes in the intensity of lignin/carbohydrate characteristic bands [22, 38, 39]. Py-GC-MS is gaining increasing interest as a fast analytical technique for the chemical analysis of degraded wood in archaeological objects, due to the minimum amount of sample needed and to the high level of detailed information achieved [40-43]. Derivatisation of pyrolysis products by *in situ* thermally assisted silylation was adopted, because it significantly improves the detectability/analytical response of polar compounds, such as some polysaccharide pyrolysis products [44], and lignin monomers bringing hydroxyl functionalities and acidic groups [29, 40]. The changes in the cellulose network were investigated by XRD; in particular, the crystallinity index of cellulose was assessed. XRD has previously enabled information to be obtained about the mechanism of cellulose degradation during short-term burial in wet conditions [35].

2. Materials and methods

2.1 Samples

Burial in wet environments: monitoring program

In 2003 two wood samples were collected from a 99-year old Scots pine (*P. sylvestris*) tree harvested from the Gołąbki Forest District, near Biskupin (Poland). The samples measured 150x10x10 mm (LxTxR) and were cutfrom wood dried to a moisture content of about 12%. After preparation, the samples were buried in two monitoring stations in the Biskupin site. One was left in a layer of wet peat (station SP1, acronym P for peat environment) at a depth of 100 cm (the level where wooden constructions were deposited). The other was placed in a peaty layer at the bottom of a pit filled with water (station SP4, acronym W for water environment). These two monitoring stations were chosen because they closely reproduce the burial conditions in which the settlement's constructions were found. Some selected water and soil parameters were previously monitored in the years 2003-2006 [1]. To minimize contamination due to direct contact with the peat and soil, the wood fragments were kept in AgroFabric® bags, thus allowing unrestricted water access. The wood samples were removed from the burial environment after different times of deposition and pieces were cut for analysis. The monitoring program (started in 2003) is still on-going and it will continue in the following years. The results presented here refer to the samples that were removed from the burial environment after 4 years and 10 years (the longest burial time to date). The samples are named here using an acronym referring to the station (P for peat and W for water) followed by a number indicating the number of

years of burial: P4, P10, W4 and W10. For example: W4 refers to wood after 4 years in water.

The results were compared with those obtained from a reference sample of the same wood used for the monitoring program (Pine Ref).

The samples were tested for resistance to biological attack according to the European Standard EN113 [45], against *C. puteana* (Schumacher ex Fries) Karstein (strain: BAM Ebw. 15) grown on malt/agar medium (malt 50g/l, agar 20g/l). All wood samples were sterilized by steam (121°C for 20min.) prior to fungal exposure. One archaeological wood sample, and a control (modern wood), was introduced in each culture vessel. The samples were incubated for 8 weeks at 22±1°C and 70±5% RH. After this the mycelium was removed and the samples were weighed to determine their moisture content at the end of fungal exposure. The samples were then dried at 103°C and their final weight was recorded. The suffix F is here used to refer to the wood samples subjected to fungal attack, and their appearance after washing is shown in Figure 2.

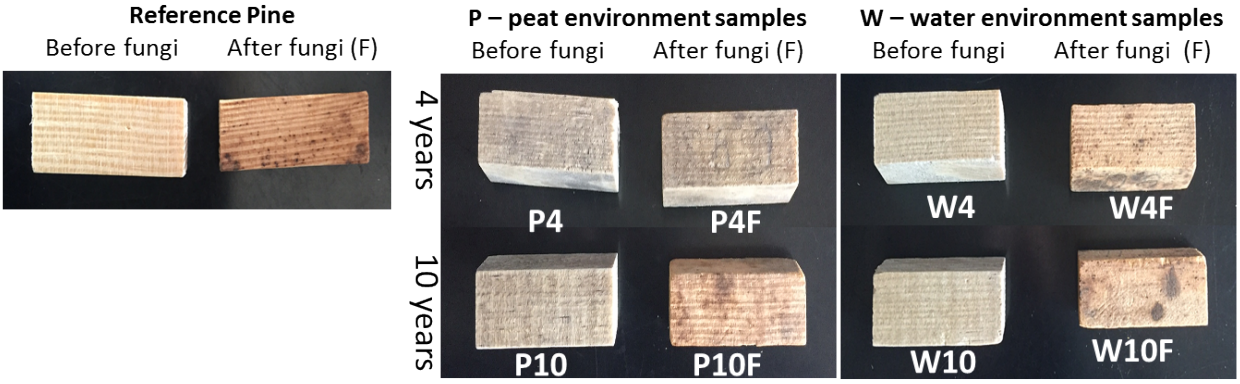

Figure 2 Pine wood samples after exposure to the brown rot fungus *C. puteana* in the laboratory for 8 weeks. P, W: provenance from the monitoring station in peat or in water, respectively. The number indicates the number of years spent in the selected environments. F: samples exposed to fungi.

2.2 SEM

The wood samples were cut to show transverse, radial longitudinal and tangential longitudinal sections (TS, RLS and TLS) prior to SEM examination.

The samples before fungal attack were investigated using a VEGA TS 5130 scanning electron microscope (Tescan, Brno, Czech Republic). The samples were sputter-coated with gold. The accelerating voltage used was between 15 and 16.7 kV. The electron source was a tungsten filament.

The samples after fungal attack were investigated uncoated using a variable pressure scanning electron microscope (VP SEM), Hitachi S-3700N. The back-scatter electron (BSE) detector was used at 15 or 20kV, with the SEM chamber partially evacuated (40 to

60Pa). The working distance (WD) ranged from 12 mm to 25 mm (as required). Using the BSE detector, 3D mode (rather than Compositional) was preferentially selected to maximize the opportunity to reveal diagnostic features.

The operating conditions (including magnification and scale bar) are recorded on the data-bar at the foot of each SEM image (Figures 3-5).

2.3 Mass Loss measurements

The percentage mass loss (ML) was calculated according to the following equation:

$$\%ML = [(Wo - Wf)/Wo] * 100$$

Wo: oven-dry weight of sample prior to fungi attack; Wf: oven-dry weight following exposure to fungi.

2.4 FTIR

FTIR spectra were obtained by means of Alfa FTIR spectrometer (Bruker Optics GmbH, Germany). 2 mg of wood samples were ground to a fine powder with a Pulverisette 23 ball mill (Fritsch, Germany). Powdered samples were dispersed in a matrix of KBr (200 mg), followed by compression to form pellets. The spectrum collection was obtained using 32 scans, in the range of 4000 to 400 cm^{-1}, at a resolution of 4 cm^{-1}. Three measurements for each wood sample were acquired, and the average value was computed.

The post-acquisition treatment of the spectra was kept to a minimum (baseline correction). To measure the height of the bands, a baseline was constructed by connecting the lowest data points on either side of the band. A vertical line from the maximum of the band to this baseline gave the band height. Ratios were calculated between band height values for lignin-associated bands against carbohydrate reference bands. These ratios provided information on the relative changes in the composition of the structural components.

2.5 Py(HMDS)-GC-MS

Analytical pyrolysis was performed using 1,1,1,3,3,3-hexamethyldisilazane (HMDS, chemical purity 99.9%, Sigma Aldrich Inc., USA) as a silylating agent for the *in situ* thermally-assisted derivatisation of pyrolysis products. The instrumentation consisted of a micro-furnace Multi-Shot Pyrolyzer EGA/Py-3030D (Frontier Lab) coupled to a gas chromatograph 6890 Agilent Technologies (USA) equipped with an HP-5MS fused silica capillary column (stationary phase 5% diphenyl- 95% dimethyl-polysiloxane, 30 m x 0.25 mm i.d., Hewlett Packard, USA) and with a deactivated silica pre-column (2 m x 0.32 mm i.d., Agilent J&W, USA). The GC was coupled with an Agilent 5973 Mass Selective Detector operating in electron impact mode (EI) at 70 eV. The pyrolysis temperature was

550 °C and interface temperature was 250 °C. Similar amounts (*ca*. 100 µg) of sample and HMDS (5 µL) were put into a stainless steel cup and inserted in the micro-furnace. Chromatographic conditions were as follows: initial temperature 50 °C, 1 min isothermal, 10 °C min^{-1} to 100 °C, 2 min isothermal, 4 °C min^{-1} to 190 °C, 1 min isothermal, 30 °C min^{-1} to 280 °C, 30 min isothermal. Carrier gas: He (purity 99.995%), constant flow 1.0 mL min^{-1}. Before being analysed, all the samples were oven dried for 24 h at 40-50 °C to remove the residual free water. After instrumental analysis, the compounds were identified by comparing their mass spectra with spectra reported in the Wiley and NIST libraries and in the literature [35, 46]. The peak areas of the most abundant pyrolysis products were normalised and expressed as percentages. The integration of identified peaks derived from lignin and holocellulose products was performed by AMDIS software, which helps to deconvolute and integrate chromatographic peaks on the basis of their mass spectra even in the presence of coelutions. Semi-quantitative calculations were performed using chromatographic areas: peak areas were normalised with respect to the sum of the peak areas of all identified pyrolysis products, and the data were averaged and expressed as percentages, in order to highlight differences in the pyrolysis yields due to degradation. The percentage areas were used to calculate the relative abundances of wood pyrolysis products divided into categories. In this case, the calculations referred to the 100% of the wood component corresponding to the considered categories. The technique has proven to achieve a relative standard deviation of 7.3% [15].

2.6 XRD

X-ray diffraction analysis was carried out using a PANalytical diffractometer X'Pert PRO with radiation CuKα1 = 1.54 Å, operating at 40 kV, 30 mA, 2θ range 3–70°, step size 0.02°, time per step 50 s, equipped with X'Celerator RTMS (Real Time Multiple Strip) X-ray detection technology, a High Score data acquisition and interpretation software. A zero background sample holder was used. A total of 8 mg of samples were used for each analysis. In order to determine the crystallinity index (CI) of the cellulose in wooden samples, the method developed by Segal et al [47] was adopted. This method calculates the CI as difference between the height of peak 200 (I_{200}) and the height of the minimum (I_{AM}) between peaks 200 and 1 $\bar{1}0$ (peaks are identified by the Miller indices [48]). The ratio between this difference and the height of the 200 peak (I_{200}) provides an estimation of the CI:

$$(I_{200} - I_{AM})/I_{200} = CI$$

The drawback of this method is that it does not take into account the width of the peaks and there is a risk of overestimating the exact CI. However, it is useful for comparing the relative differences between samples [49-51]. The non-aged sample was analysed in triplicate and the result was CI = 0.70 ± 0.01. This low standard deviation was taken as an indication of the good reproducibility of the technique.

3 Results

The interpretation of the results was based on the comparison of three types of samples: reference pine sound wood (Ref Pine), wood buried in wet (peat or water) environments for 4 and 10 years (P4, P10, W4, W10), and wood exposed to fungal attack after burial (Ref Pine F, P4F, P10F, W4F, W10F). The contextual evaluation of the observed changes has enabled conclusions to be drawn on the alterations induced both during the burial period and by fungal action.

3.1 SEM

Scanning electron microscopy provides an informative tool to examine and investigate morphological changes resulting from wood decay processes. Our first investigative approach to pine wood after burial in the wet environments and after treatment with fungi was the examination of the transverse sections (TS).

By comparing sound wood with wood from the monitoring stations in peat and in lake water, a range of morphological and anatomical alterations was observed. In particular, for the reference wood the cell walls of the axial tracheids appeared homogeneously thick, intact and compact in both the earlywood and the latewood (Figure 3a). a An almost perfect cell wall structure was revealed at high magnification, where the lignin-rich middle lamella was clearly visible between the tracheids and was always in contact with the cell walls, which did not show any sign of alteration (Figure 3b). After four years of burial in peat (sample P4), the main change affected some areas of the latewood, where the S_2 layer of the cell walls of the tracheids appeared altered (Figure 3c). The exact cause of this phenomenon was not clear. However, some fungal spores were present and the pattern is partially compatible with brown rot fungal decay [9]. An attack by brown rot fungi may have started in the 99 year old reference wood sample, although clear evidence was not forthcoming based on the SEM images acquired. A similar phenomenon was observed in sample W4. In addition, for this sample, there was remarkable distortion of the cell walls in the earlywood (Figure 3d). This may be due to shrinkage of the wood after removal from water. For samples P10 and W10 the extent of the alteration increased (Figures 3e and 3f). A complete detachment of the cell walls from the middle lamella was visible in some areas and the cell walls were completely absent in some cases. It was interesting to observe that the phenomenon was present only in some areas, whereas others showed a perfect preservation condition.

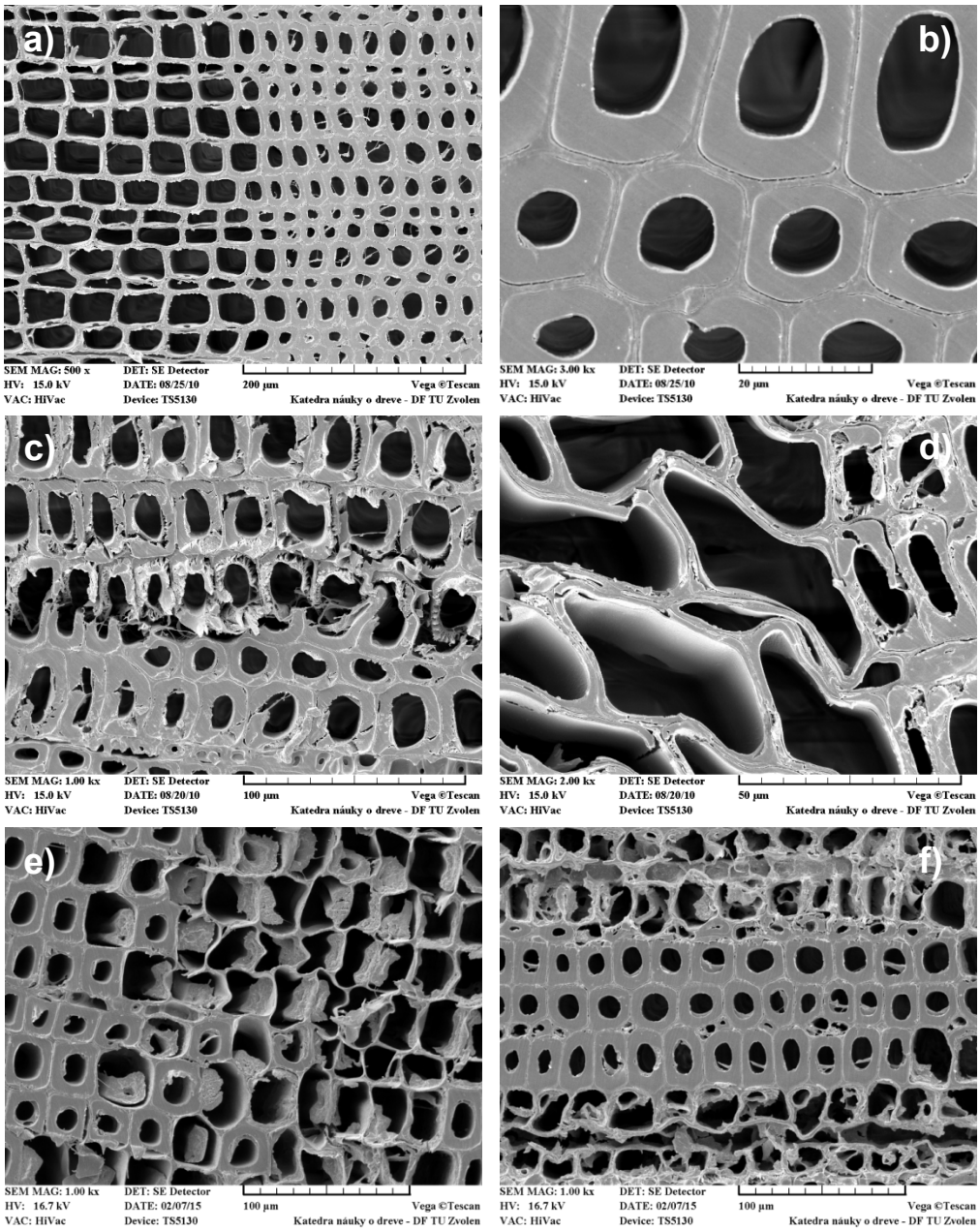

Figure 3. Scanning electron microscope images of gold-coated TS of **a, b)** Ref pine, **c)** sample P4, **d)** sample W4, **e)**, sample P10 and **f)** sample W10

The TS of the reference pine sample after fungal attack showed the formation of irregularities and cavities mainly affecting the S_2 layer of the axial tracheid walls in both the latewood (Figure 4a) and the earlywood. The degradation pattern, especially the deformation of the cell walls, is consistent with brown rot decay, although the shape of the cavities can also sometimes be indicative of a soft rot type of decay [9]. Similar observations have already been reported for *C. puteana* [52]. In addition, the TS also displayed the abundant presence of fungal hyphae in the resin canals and in most of the cell lumens of the axial tracheids (Figure 4b), showing that the fungus follows these routes preferentially to spread into the wood structure.

Similar features were observed for samples P4F and W4F. The cell walls of the axial tracheids in the TS showed the same signs of degradation as in the reference sample (Figures 4c and 4d). Similarly to what was observed for the samples not attacked by fungi, the alterations seemed to involve some areas more than others.

Samples P10F and W10F were generally in worse condition. Cavities in the S_2 layer of the cell walls were dispersed in the TS, indicating an advanced stage of fungal attack compared to the other samples (Figures 4e and 4f). The structure of the axial tracheids appeared highly disrupted where fungal hyphae were present.

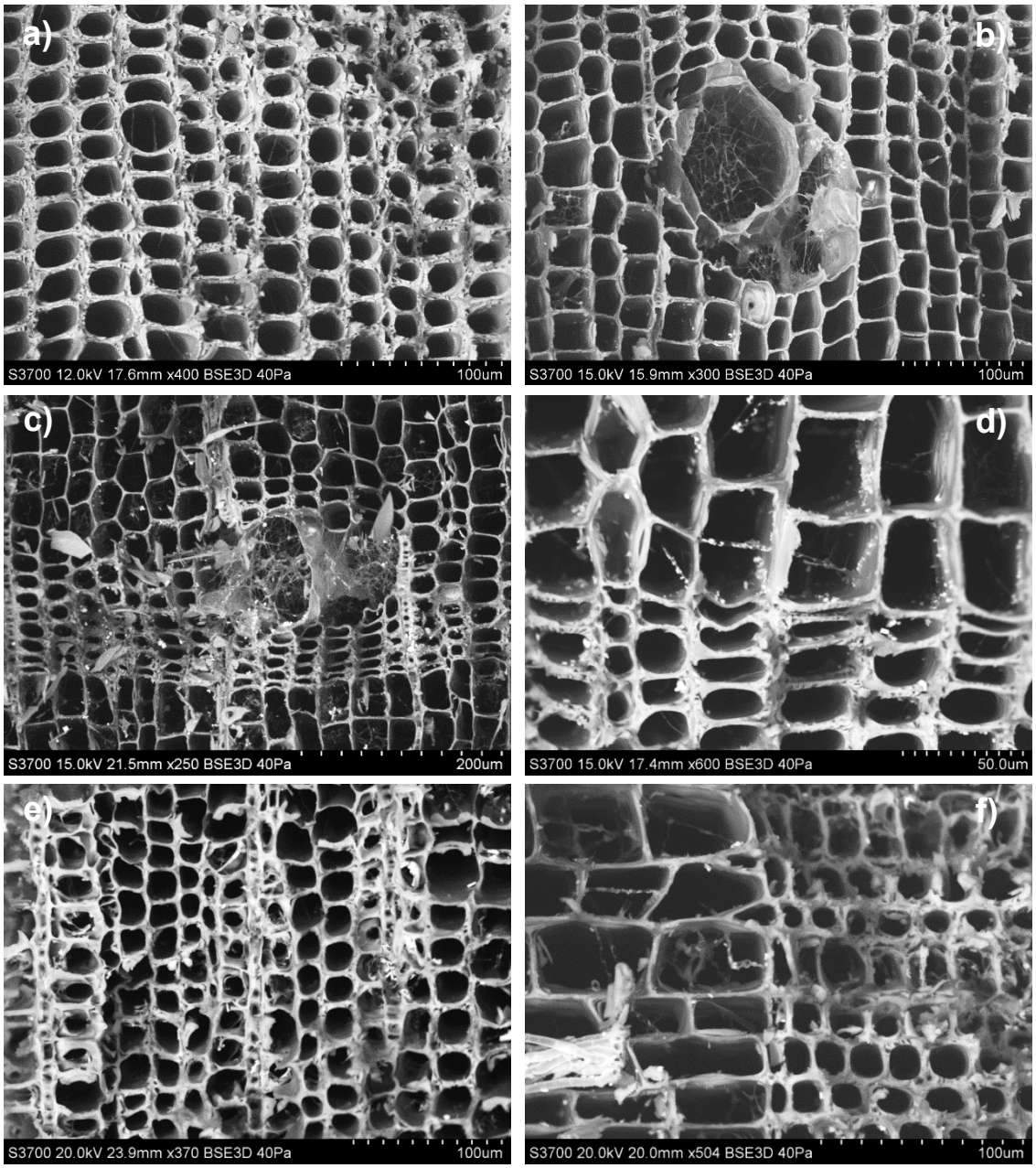

346 **Figure 4**. Variable pressure scanning electron microscope images of uncoated TS of **a, b)**
347 pine reference wood after fungal attack, **c)** sample P4F, **d)** sample W4F, **e)**, sample P10F
348 and **f)** sample W10F. Images © The Trustees of the British Museum

349

350

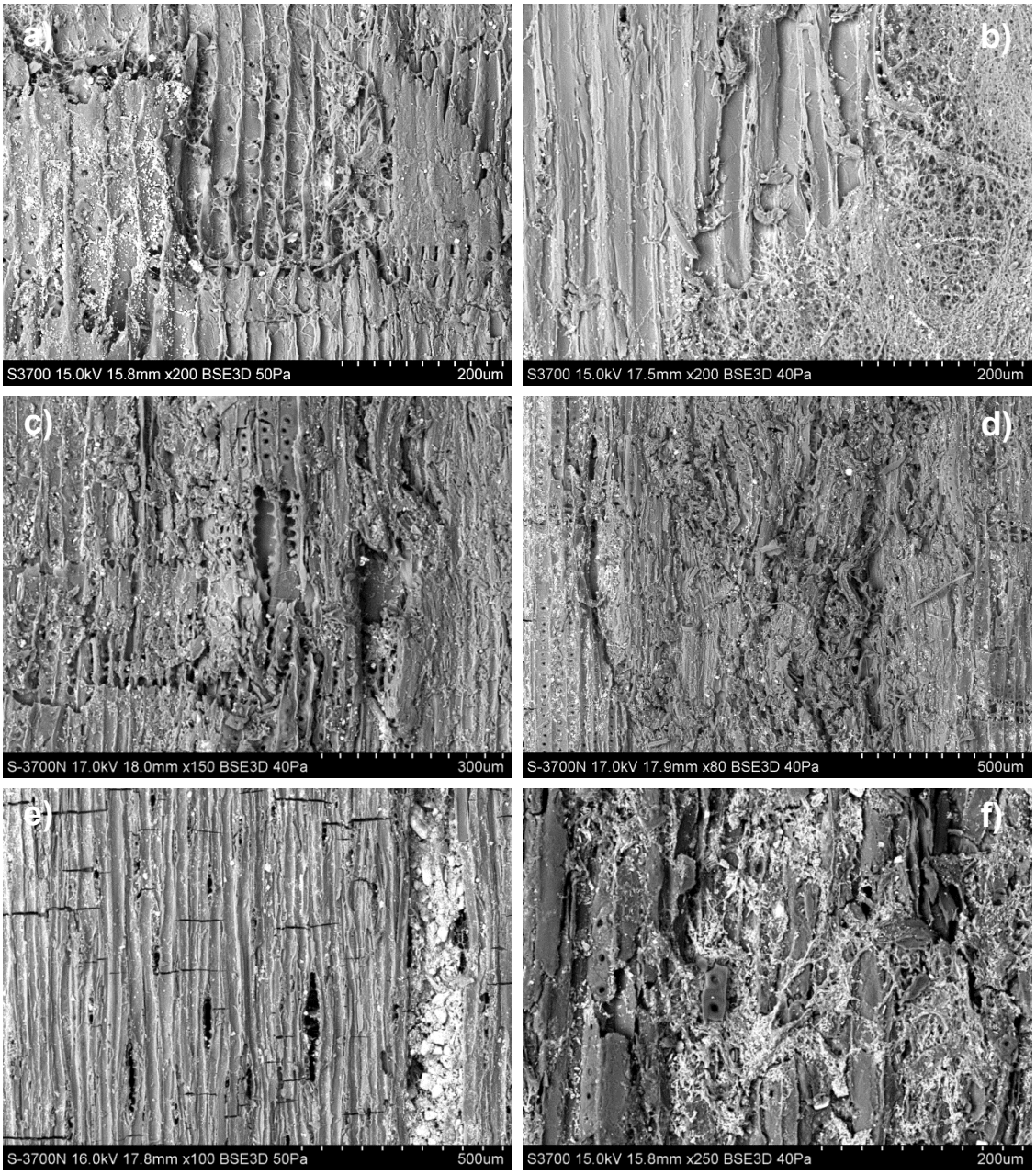

351

352 **Figure 5.** Variable pressure scanning electron microscope images of uncoated **a)** RLS of
353 pine reference after fungal attack, **b)** TLS of pine reference after fungal attack, **c)** RLS of
354 sample P10F, **d)** RLS of sample W10F, **e)** TLS of sample P10F and **f)** TLS of sample
355 W10F. Images © The Trustees of the British Museum.

356

In addition to the TS, useful information was obtained from radial longitudinal (RLS) and tangential longitudinal (TLS) sections. In fact, fungal hyphae appear to cover large areas of the RLS of the reference pine (Figure 5a), highlighting the widespread presence of the fungus in the cell lumen of the axial tracheids. Hyphae were also observed to grow across and into the bordered axial tracheid pits and the rays, thus penetrating adjacent cells. As a consequence, some of the axial tracheid pits showed a slight alteration of the edges, which appeared rather irregular. In the TLS of the pine reference the fungal hyphae were generally present in patches on the surface of the axial tracheids (Figure 5b). However, where resin canals are present, these were readily populated by hyphae, as these represented an easy route into the wood. In the areas not covered by hyphae, no specific degradation signs were observed in the TLS, whereas where hyphae were present, disruption of the axial tracheid walls can be seen.

An increasing trend for morphological alteration was highlighted for samples P4F and W4F and samples P10F and W10F. The main changes were related to the border of the axial tracheid pits in RLS (Figure 5c), which appeared irregular and in some cases slightly raised; and perpendicular cracks were often visible in the TLS, probably ascribable to the swelling of the wood (in water) and subsequent drying out (Figure 5e). Under close examination, the cell walls of the uniseriate rays visible in the TLS appeared broken or absent (Figure 5e). All these phenomena were particularly advanced after ten years of burial in the wet environments. Additionally, the surface of the wood appeared highly disrupted in some areas where fungal hyphae were present (Figures 5d and 5f), thus masking most of the wood anatomical features. The hyphae covered large areas of the wood sections and penetrated deeply beneath the surface. Abundant perpendicular cracks were observed in the TLS.

3.2 Measurements of mass loss

The mass loss of the wood samples during the fungal attack was measured. The results showed that the action of fungi caused a mass loss ranging from 15 to 25 % in all the samples. Figure 6 shows that the mass loss caused by brown rot fungi is dependent on the state of degradation of the wood substrate. The fungi caused a mass loss of 24.5 % for the sample of sound pine wood (Pine Ref), whereas the samples which have undergone burial in wet peat and in water were less consumed by fungi. For sample P4F the mass loss during fungal attack was 19.8 %, whereas for sample P10F it was 19.0. For sample W4F the mass loss was 16.2 %, whereas for sample W10F it was 15.2 %. Consequently, the mass loss caused by fungi was more significant for sound wood than for degraded wood.

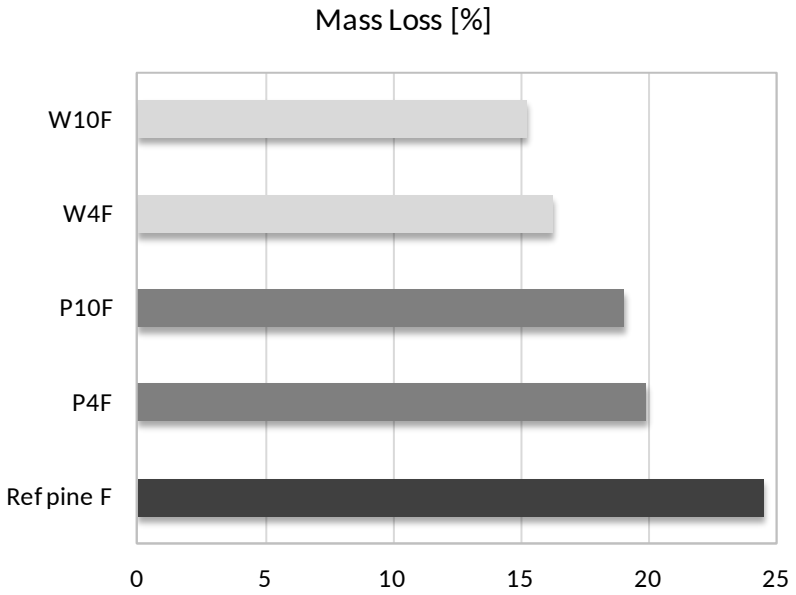

Figure 6. Mass loss expressed as a percentage (average of 10 replicates) exhibited by reference pine wood (Ref Pine F) and by pine wood naturally aged in water (W) and in peat (P) for 4 and 10 years during attack by brown rot fungi *C. puteana.*

3.3 FTIR

The FTIR spectrum in the fingerprint region (2000-400 cm^{-1}) of reference pine wood is shown in Figure 7. Most of the bands have contributions from all the wood components. Only a few bands can be purely attributed to carbohydrates or lignin [22, 38, 39]. The band at 1730 cm^{-1} is assigned to C=O stretching in unconjugated ketones, carboxyl and ester groups (mainly from hemicelluloses) [22] and its progressive decrease in intensity for the buried samples can be taken as a qualitative indication of degradation involving hemicelluloses during the years of burial. The band at 1508 cm^{-1}, is due to aromatic skeletal vibration (C=C) in lignin [22, 39].

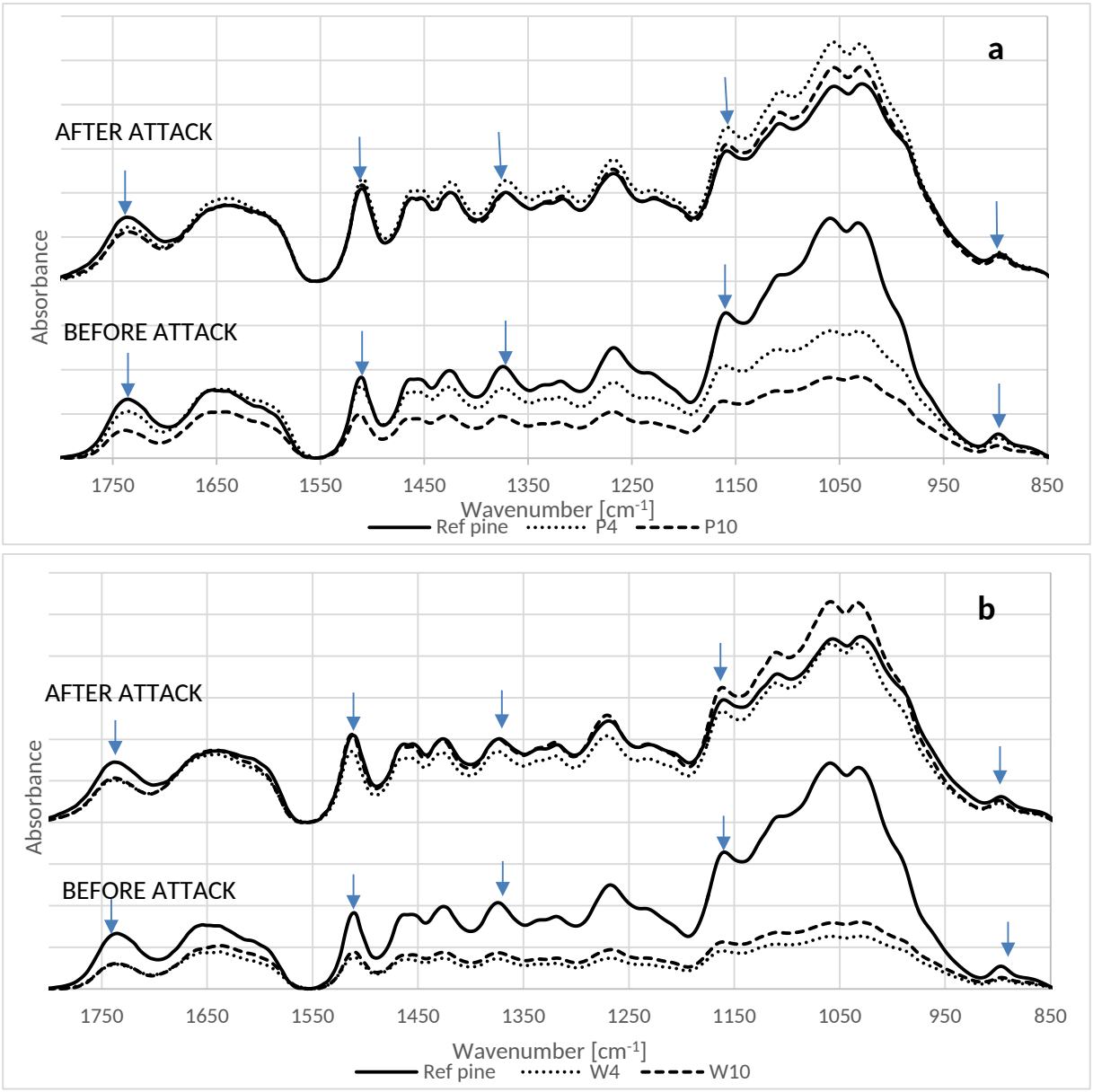

Figure 7. FTIR spectrum of reference pine wood (Ref pine) and samples buried in peat **(a)** and in water **(b)**, before and after fungal attack.

In order to highlight differences in the intensities of absorption bands more effectively, some semi-quantitative calculations were performed, following the method presented by Pandey [22]. The results are presented in Figure 8. The ratios between the relative intensities of the lignin band at 1508 cm^{-1} against the carbohydrate bands at 1730, 1370, 1155 and 897 cm^{-1} were calculated using band heights (see section 2.4). All carbohydrate bands used for calculations have no significant contribution from lignin [22, 38, 39] and they are attributed to:

- 1730 cm^{-1} stretching of unconjugated C=O in xylans (hemicelluloses),
- 1370 cm^{-1} C–H deformation in cellulose and hemicelluloses (holocellulose),
- 1155 cm^{-1} C–O–C vibration in cellulose and hemicelluloses (holocellulose),
- 897 cm^{-1} C–H deformation in cellulose.

425 Calculations were also undertaken to observe the relative changes in cellulose and
426 hemicelluloses, the ratio between the band relative only to hemicelluloses (at 1730 cm^{-1})
427 and that relative only to cellulose (at 897 cm^{-1})

428 When comparing the degraded samples with the reference wood, an increase in the first
429 four calculated ratios can be taken as an indication of a slight depletion of the
430 carbohydrates during ten years of burial. In particular, the increase in the ratios 1508/1730
431 (lignin/hemicelluloses) and 1508/1155 (lignin/holocellulose) and the unspecific trend of the
432 ratio 1508/897 (lignin/cellulose) can be regarded as an indication that the chemical
433 changes occurring in the waterlogged environments mainly involved hemicelluloses, which
434 are more prone to hydrolysis than cellulose [53-55]. The higher extent of degradation of
435 hemicelluloses with respect to cellulose during the time spent in both peat and lake water
436 has also been confirmed by the decrease in the ratio 1730/897 (hemicelluloses/cellulose).
437 For the samples buried in water the ratios 1508/1730, 1508/1155 and 1730/897
438 significantly changed with respect to the wet peat environment (P), indicating that the
439 degradation processes of carbohydrates occur to a greater extent in water than in peat.

440

441

442

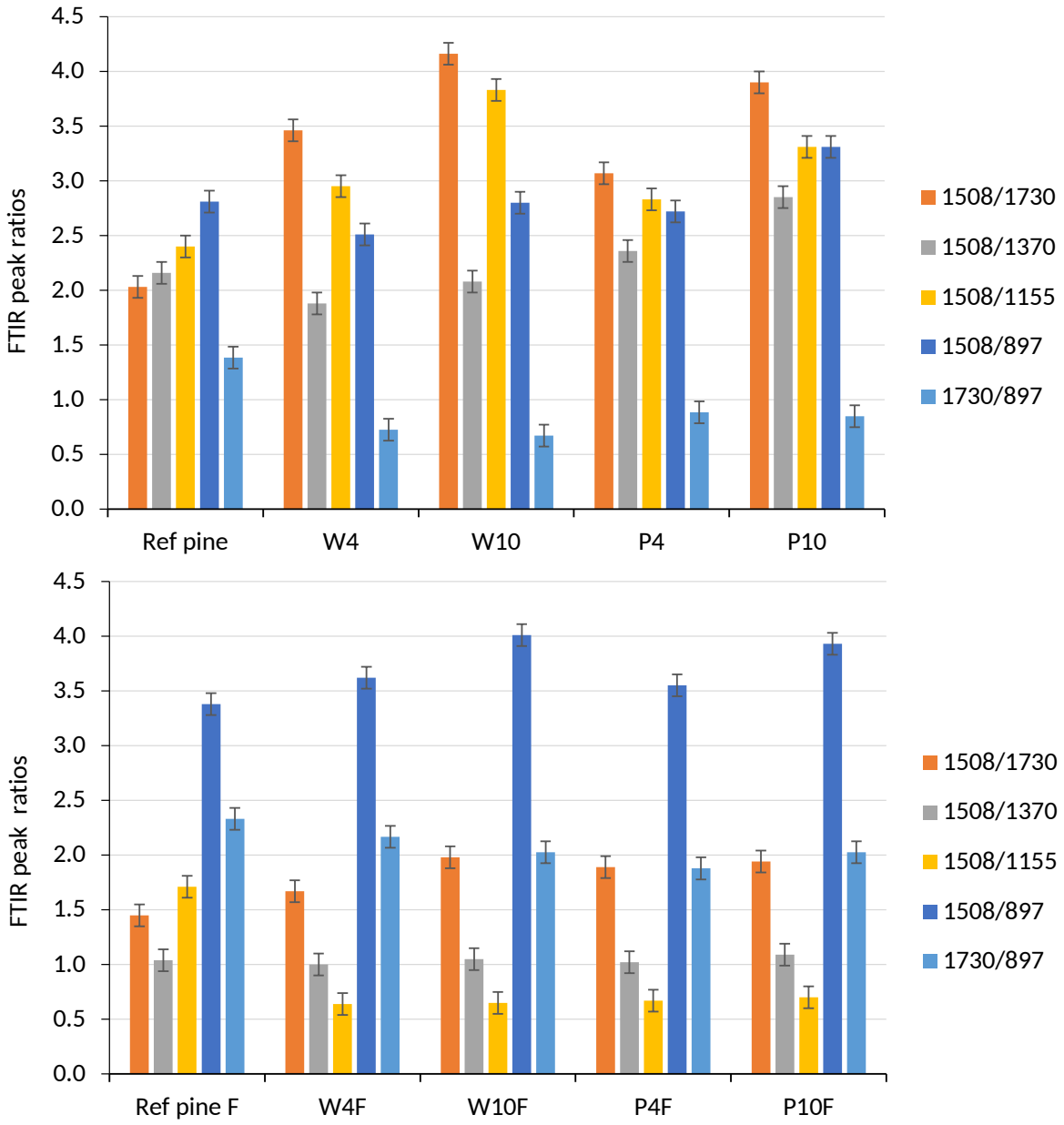

Figure 8. Histograms showing the values of the ratios calculated between the selected FTIR band heights for the samples from **(a)** lake water and **(b)** peat environments before and after fungal attack. Selected absorption bands: 1508 cm^{-1}: lignin; 1730 cm^{-1}: hemicelluloses C=O stretching; 1370 cm^{-1}: cellulose and hemicelluloses C–H deformation; 1155 cm^{-1}: cellulose and hemicelluloses C–O–C vibrations; 897 cm^{-1}: cellulose C–H deformation.

The examination of the FTIR spectra of the wood fragments after exposure to brown rot fungus *C. puteana* for 8 weeks highlighted some significant variations in comparison to the spectra before fungal action, which can be related to chemical alterations, as shown in Figure 8.

After the exposure to fungal attack the lignin/cellulose ratios (1508/897) strongly increased, highlighting a depletion of cellulose in all analysed samples. This result, together with the significant decrease in the other lignin/carbohydrate ratios (1508/1730, 1508/1370 and 1508/1155), suggested that in the adopted conditions the fungus preferentially attacks the cellulose with respect to the hemicelluloses. This trend has also been confirmed by the increase in the hemicelluloses/cellulose ratio (1730/897).

FTIR spectra highlighted that the effect produced by the fungal attack is different from that of the wet environments on the polysaccharides present in the wood. The wet environments caused changes mostly in the hemicelluloses, whereas the fungal attack was mainly directed towards cellulose degradation.

3.4 Py-GC-MS

When wood is pyrolysed and the pyrolysis products analysed by gas chromatography mass spectrometry, a pyrolytic chromatographic profile is obtained in which pyrolysis products of lignin, cellulose and hemicelluloses can be identified thanks to their mass spectra [40]. Figure 9 shows the pyrograms obtained in the Py-GC-MS analysis of the pine wood samples after 4 and 10 years of burial in wet peat (samples P4 and P10 respectively), compared with the reference pine wood. The pyrolysis products can be attributed to holocellulose (H) and guaiacyl-lignin (L). Table 1 reports a list of 90 identified compounds. Some pyrolysis products are marked as “unknown”. In fact, the molecular structures of these compounds were not disclosed. Nevertheless, the analysis of reference holocellulose and lignin samples enabled these compounds to be attributed to the correct wood component [32, 35, 56].

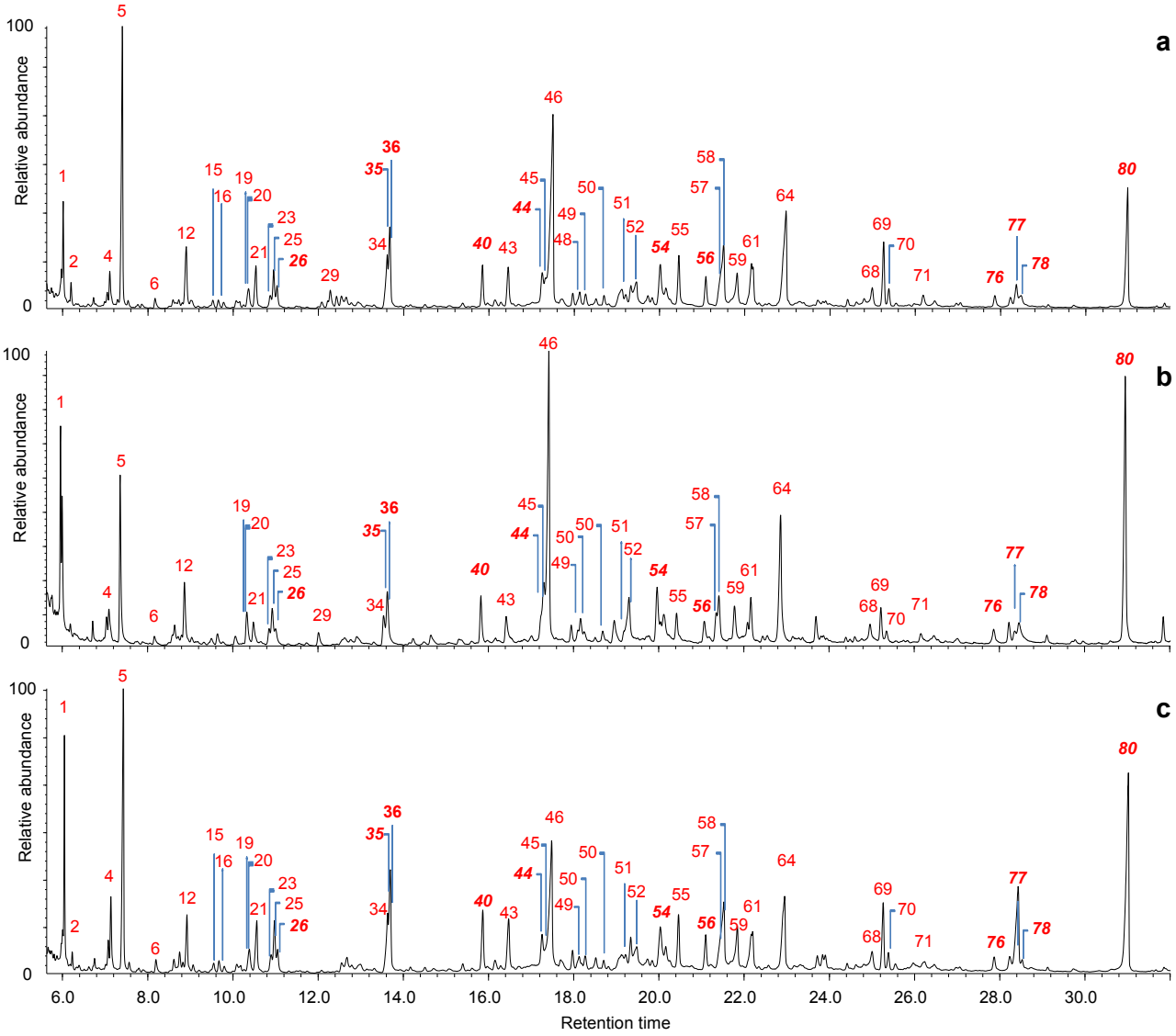

Figure 9. Py(HMDS)-GC-MS chromatographic profiles of **a)** reference pine wood (Pine Ref), **b)** sample P4, **c)** sample P10. Peak labelling refers to Table 1. In Italic: lignin pyrolysis products.

Table 1. List of wood pyrolysis products identified by Py(HMDS)-GC-MS, divided into categories. H-Holocellulose, L-Lignin, Smo- small molecules, Cyp-cyclopentenones, Pyr-pyrans, Fur-furans, Hyb-hydroxybenzenes, Ahs-anhydrosugars, Mon-monomers, Cre-cresols, Oxd-oxidized, Sho-short chain, Dem-demethylated/demethoxylated compounds, Oth-others.

#	Name	Origin	Cat
1	1,2-dihydroxyethane (2TMS)		Smo
2	2-hydroxymethylfuran (TMS)	H	Fur
3	phenol (TMS)	L	Cre
4	2-hydroxypropanoic acid (2TMS)		Smo
5	2-hydroxyacetic acid (2TMS)		Smo
6	1-hydroxy-1-cyclopenten-3-one (TMS)	H	Cyp
7	3-hydroxymethylfuran (TMS)	H	Fur
8	o-cresol (TMS)	L	Cre
9	2-furancarboxylic acid (TMS)	H	Fur
10	unknown I	H	Oth
11	m-cresol (TMS)	L	Cre
12	2-hydroxy-1-cyclopenten-3-one (TMS)	H	Cyp
13	p-cresol (TMS)	L	Cre
14	3-hydroxy-(2H)-pyran-2-one (TMS)	H	Pyr
15	unknown II	H	Oth
16	unknown III	H	Oth
17	Z-2,3-dihydroxy-cyclopent-2-enone (TMS)	H	Cyp
18	E-2,3-dihydroxy-cyclopent-2-enone (TMS)	H	Cyp
19	1,2-dihydroxybenzene (TMS)	H	Hyb
20	3-hydroxy-(4H)-pyran-4-one (TMS)	H	Pyr
21	5-hydroxy-2H-pyran-4(3H)-one (TMS)	H	Pyr
22	2-hydroxymethyl-3-methy-2-cyclopentenone (TMS)	H	Cyp
23	1-hydroxy-2-methyl-1- cyclopenten-3-one (TMS)	H	Cyp
24	1-methy-2-hydroxy-1-cyclopenten-3-one (TMS)	H	Cyp
25	1,3-dihydroxyacetone (2TMS)		Smo
26	guaiacol (TMS)	L	Shc
27	unknown IV	H	Oth
28	3-hydroxy-6-methyl-(2H)-pyran-2-one (TMS)	H	Pyr
29	unknown V	H	Oth
30	2-methyl-3-hydroxy-(4H)-pyran-4-one (TMS)	H	Pyr
31	2-methyl-3-hydroxymethyl-2-cyclopentenone (TMS)	H	Cyp
32	2,3-dihydrofuran-2,3-diol (2TMS)	H	Fur
33	2-furyl-hydroxymethylketone (TMS)	H	Fur
34	5-hydroxymethyl-2-furaldehyde (TMS)	H	Fur
35	4-methylguaiacol (TMS)	L	Shc
36	1,2-dihydroxybenzene (2TMS)	H	Hyb
37	2-hydroxymethyl-2,3-dihydropyran-4-one (TMS)	H	Pyr
38	1,4:3,6-dianhydro-α-D-glucopyranose (TMS)	H	Ahs
39	Z-2,3-dihydroxy-cyclopent-2-enone (2TMS)	H	Cyp
40	4-methylcatechol (2TMS)	L	Dem
41	4-ethylguaiacol (TMS)	L	Shc

42	1,4-dihydroxybenzene (2TMS)	H	Hyb
43	arabinofuranose (4TMS)	H	Oth
44	4-vinylguaiacol (TMS)	L	Shc
45	3-hydroxy-2-hydroxymethyl-2-cyclopentenone (2TMS)	H	Cyp
46	E-2,3-dihydroxy-cyclopent-2-enone (2TMS)	H	Cyp
47	4-ethylcatechol (2TMS)	L	Dem
48	3-hydroxy-2-(hydroxymethyl)cyclopenta-2,4-dienone (2TMS)	H	Cyp
49	eugenol (TMS)	L	Lch
50	3,5-dihydroxy-2-methyl-(4H)-pyran-4-one (2TMS)	H	Pyr
51	1,6-anydro-beta-D-glucopyranose (TMS at position 4)	H	Ahs
52	1,6-anydro-beta-D-glucopyranose (TMS at position 2)	H	Ahs
53	Z-isoeugenol (TMS)	L	Lch
54	vanillin (TMS)	L	Car
55	1,2,3-trihydroxybenzene (3TMS)	H	Hyb
56	E-isoeugenol (TMS)	L	Lch
57	1,4-anydro-D-galactopyranose (2TMS)	H	Ahs
58	1,6-anydro-D-galactopyranose (2TMS)	H	Ahs
59	2-hydroxymethyl-5-hydroxy-2,3-dihydro-(4H)-pyran-4-one (2TMS)	H	Pyr
60	1,4-anydro-D-glucopyranose (2TMS at position 2 and 4)	H	Ahs
61	1,2,4-trihydroxybenzene (3TMS)	H	Hyb
62	acetovanillone (TMS)	L	Car
63	4-hydroxy benzoic acid (2TMS)	L	Acd
64	1,6-anydro-beta-D-glucopyranose (2TMS at position 2 and 4)	H	Ahs
65	vanillic acid methyl ester (TMS)	L	Est
66	1,4-anydro-D-galactopyranose (3TMS)	H	Ahs
67	unknown lignin 416	L	Oth
68	2,3,5-trihydroxy-4H-pyran-4-one (3TMS)	H	Pyr
69	1,6-anydro-beta-D-glucopyranose (3TMS)	H	Ahs
70	1,4-anhydro-D-glucopyranose (3TMS)	H	Ahs
71	1,6-anydro-beta-D-glucofuranose (3TMS)	H	Ahs
72	unknown lignin 430	L	Oth
73	unknown lignin 416 II	L	Oth
74	vanillic acid (2TMS)	L	Acd
75	coumaryl alcohol (2 TMS)	L	Dem
76	vanillylpropanol (2TMS)	L	Lch
77	Z-coniferyl alcohol (2 TMS)	L	Mon
78	coniferylaldehyde (TMS)	L	Car
79	unknown lignin 340	L	Oth
80	E-coniferyl alcohol(2 TMS)	L	Mon
81	unknown lignin 340 II	L	Oth
82	3,4-dihydroxy cinnamyl alcohol (3TMS)	L	Dem
83	unknown lignin 370	L	Oth
84	unknown anhydrosugar I	H	Ahs
85	unknown anhydrosugar II	H	Ahs
86	unknown anhydrosugar III	H	Ahs
87	unknown anhydrosugar IV	H	Ahs
88	unknown anhydrosugar V	H	Ahs
89	unknown anhydrosugar VI	H	Ahs

90	unknown anhydrosugar VII	H	Ahs

As noted already, the evaluation of the degradation state of wood is based on the comparison between waterlogged/degraded and sound wood of the same species. The holocellulose (cellulose and hemicelluloses) versus lignin ratio (H/L) is widely recognised as a fundamental chemical parameter to evaluate the decay of waterlogged/degraded (archaeological) wood. The preferential depletion of polysaccharides as an effect of hydrolysis and of the action of anaerobic bacteria in waterlogged environments is one of the main degradation processes described in the literature [40].
The results of the calculation of the H/L ratios from Py-GC-MS data are presented in Table 2. The pyrolytic H/L ratio was 2.6 for the sound reference pine. With regard to the samples before fungal attack, in the case of peat, the H/L decreased during the 10 years of deposition from 2.6 to 2.1. A similar trend was observed in the case of water, with a final H/L value 1.8, indicating that the degradation processes of carbohydrates occurred at a higher degree in water than in peat, as also observed by FTIR analysis. The increase in the H/L ratio for sample P10 compared to sample P4 was probably due to an increase in the pyrolysis yield of carbohydrates. In fact, when part of the glycosidic bonds is already cleaved by depolymerisation, the pyrolysis thermal degradation is more efficient, with the final outcome of an increase in the pyrolysis yield for carbohydrates [44].

Table 2. Pyrolytic holocellulose versus lignin ratio (H/L) determined for the pine wood samples deposited in wet peat (P) and lake water (W) in the Biskupin site before and after brown rot fungal attack.

	Before fungal attack				
	Ref pine	**W4**	**W10**	**P4**	**P10**
H/L	2.6	1.8	1.8	1.6	2.1
	After fungal attack				
	Ref pine F	**W4F**	**W10F**	**P4F**	**P10F**
H/L	1.3	1.6	2.0	1.3	1.5

With regard to the samples after fungal attack, fungi caused a further degradation of wood involving polysaccharides, as shown by the general decrease in the H/L values compared to the samples before fungal attack (Table 2). The decrease was more significant for sound wood than for naturally-degraded wood. This result was consistent with the mass loss data, which suggested in some way, that sound wood is more easily consumed or attacked by fungi than degraded wood. This can be partially explained by the varying availability of non-degraded polysaccharides in the samples.

In order to obtain more detailed information about the degradation processes occurring in wood polymers, pyrolysis products were divided into categories based on the structure and mechanisms that lead to their formation [35, 57-59]. Semi-quantitative calculations were

performed on the integrated peak areas obtained from the pyrograms (see section 2.5); the results are reported in Figures 10 and 11.

Holocellulose pyrolysis products were divided into six categories: small molecules (Smo), cyclopentenones (Cyp), pyrans (Pyr), furans (Fur), hydroxybenzenes (Hyb) and anhydrosugars (Ahs). Generally, the cleavage of the glycosidic bonds in polysaccharides generates dehydrated monosaccharides, which can evolve into different products following competitive mechanisms. The formation of an intramolecular C-O-C bond leads to the formation of anhydrosugars (Ahs), which are well-known pyrolysis products of cellulose and hemicelluloses [35, 44]. However, the loss of one or more water molecules favours the formation of products with conjugated double bonds such as pyrans (Pyr) and furans (Fur). The ring-opening of the dehydrated monomer, followed by the formation of a C-C bond, leads to the formation of cyclopentenones (Cyp) and hydroxybenzenes (Hyb). Finally, extrusion, rearrangement and secondary degradation reactions can generate small molecules with 1 to 3 carbon atoms (Smo) [35, 57].

Lignin pyrolysis products were divided into five categories: intact monomers (Mon), cresols (Cre), oxidation products (Oxd), shortened chain products (Sho) and demethylation/demethoxylation products (Dem) [32]. The most common pyrolytic reactions involve cleavage of the C-C bonds on the alkyl chains attached to the aromatic moiety of lignin monomers (Mon). The alkyl chains may be shortened or completely removed by these reactions (Sho). Radical oxidation of the C-O bonds can take place when the bonds between monomers are cleaved, and carbonyl or carboxyl moieties are obtained (Oxd). Finally, demethylation reactions may occur on the methoxy moieties, generating demethylated monomers or catechol-like products (Dem). When both demethylation and alkyl chain loss take place, cresol-like structures are obtained (Cre) [58, 59].

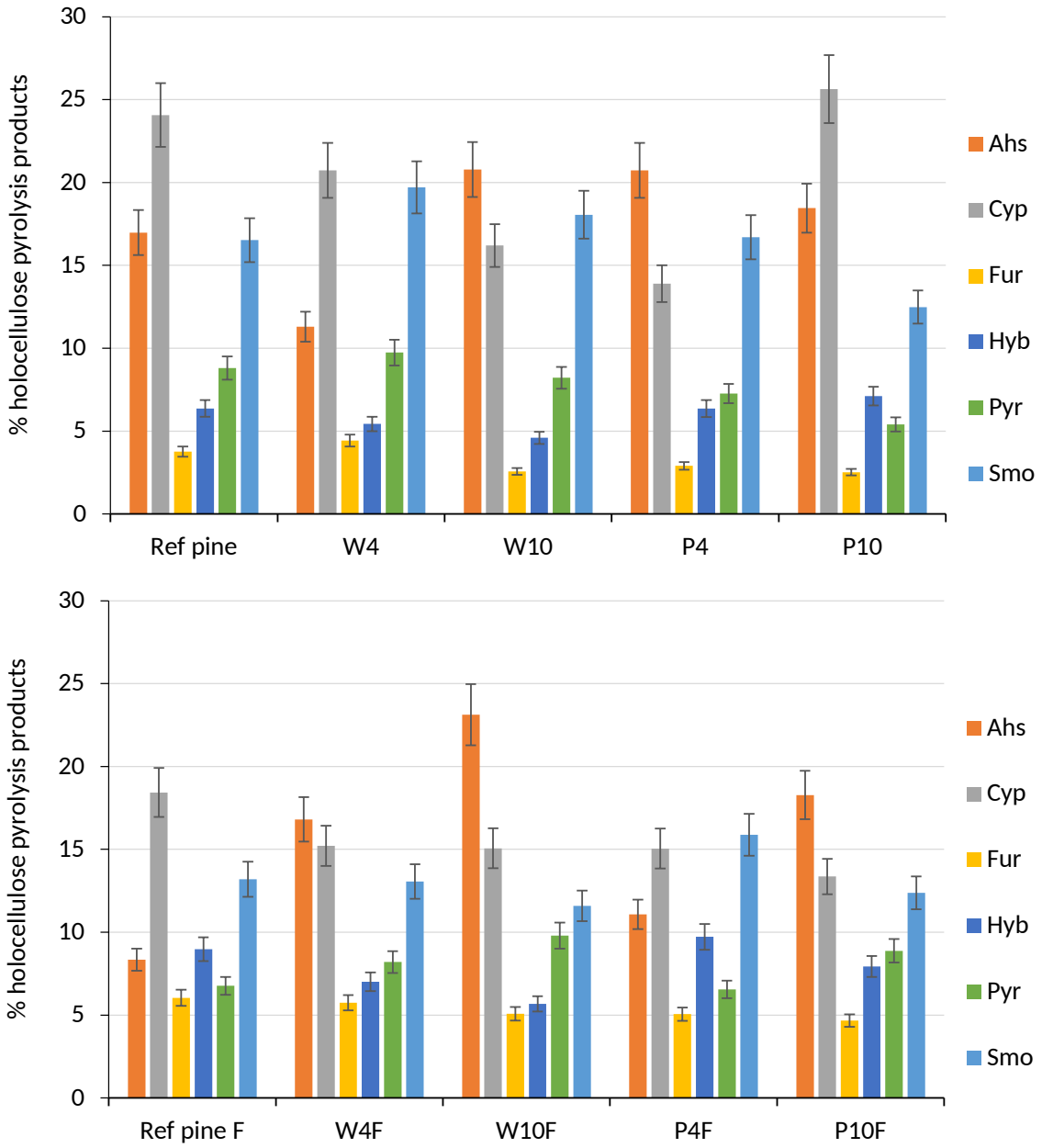

552

553 **Figure 10.** Distribution of categories of holocellulose pyrolysis products expressed as
554 percentages for the samples before **(a)** and after **(b)** fungal attack.

555

556 The most abundant groups of holocellulose pyrolysis products in sound wood are
557 generally cyclopentenones (Cyp), in particular due to the formation of 3-hydroxy-2-
558 hydroxymethyl-2-cyclopentenone (2TMS) and *E*-2,3-dihydroxy-cyclopent-2-enone (2TMS),
559 and the second most abundant group is composed of anhydrosugars (Ahs) with
560 levoglucosan (1,6-anydro-beta-D-glucopyranose) being the main product [32]. It is known
561 that during the pyrolysis of degraded wood the polysaccharides tend to form mainly
562 anhydrosugars (Ahs), whose increase in abundance is considered as an index of
563 depolymerisation of polysaccharides, because they formed preferentially when the
564 polymer has a more open structure and lower molecular weight [32, 57].

The samples aged in the two wet environments (Figure 10a) showed different changes in holocellulose pyrolysis products, probably due to different burial conditions, such as pH (7.8 in lake water and 6.9 in peat) or conductivity (0.6 in water and 1.5 mS/cm in peat) [1]. In the samples buried in lake water the degradation of holocellulose associated with the increase in the relative amount of anhydrosugars (Ahs) with respect to reference pine wood was observed only after 10 years, whereas this was visible in the samples buried in peat after 4 years. Cyclopentenones showed a tendency to decrease in all samples except for sample P10. This result is quite difficult to explain just on the basis of these results.

After fungal attack (Figure 10b) further relative increases in the abundance of anhydrosugars and slight relative decrease in cyclopentenones were observed with respect to samples before the treatment (Figure 10a). The fungi caused a further alteration of the polymeric polysaccharide network in the wood already degraded by the wet environment. Alteration processes occurring in wood samples as an effect of fungi can also be observed from the relative increase in other holocellulose pyrolysis products, such as hydroxybenzenes (Hyb), furans (Fur) and pyranes (Pyr).

The results for the lignin pyrolysis products before and after fungal attack are shown in Figure 11. The most abundant lignin pyrolysis groups in the reference pine sample are monomers (Mon), *Z*- and *E*-coniferyl alcohols. Their relative abundance did not show a clear trend of variation during natural ageing because this category appeared reduced for sample W4, whereas a slight increase was observed for the other samples (Figure 11a). In addition, a decrease was highlighted in the short side chain aromatic molecules (Sho), produced by secondary pyrolysis reactions.,.

After fungal attack (Figure 11b), there was a noticeable relative decrease in monomers and an increase in the short side chain aromatic molecules (Sho). The abundance of Sho, such as guaiacol (#26), can be considered as an index of lignin degradation. The increase in the yield for secondary reactions may be related to a less compact and less reticulated lignin structure, which is relatively more susceptible to undergo further pyrolytic degradation. This cannot be linked directly to lignin degradation, which is known to be quite stable in waterlogged condition [54], however it is likely to be the result of a cleavage of carbohydrate-lignin bonds induced by fungal action. The partial cleavage of these bonds allowed thermal energy not only to break the inter-monomeric bonds, but also other bonds, resulting in the increase in lignin pyrolysis products with a short side chain.

Another class of lignin pyrolysis products whose abundance can be interpreted as an index of degradation is represented by phenols containing a carbonyl or carboxyl group in the side chain, such as vanillin, syringaldehyde, vanillic acid or syringic acid. These compounds are produced with very small relative abundances from sound lignin. Thus, the increase in carbonyl or carboxyl functionalities in pyrolysis products indicated that these functional groups were produced in the lignin structure due to oxidative processes. With respect to the reference sample, all the wood samples attacked by fungi showed higher relative abundances of carbonyl and carboxyl compounds (Oxd), thus indicating a slight degree of lignin oxidation.

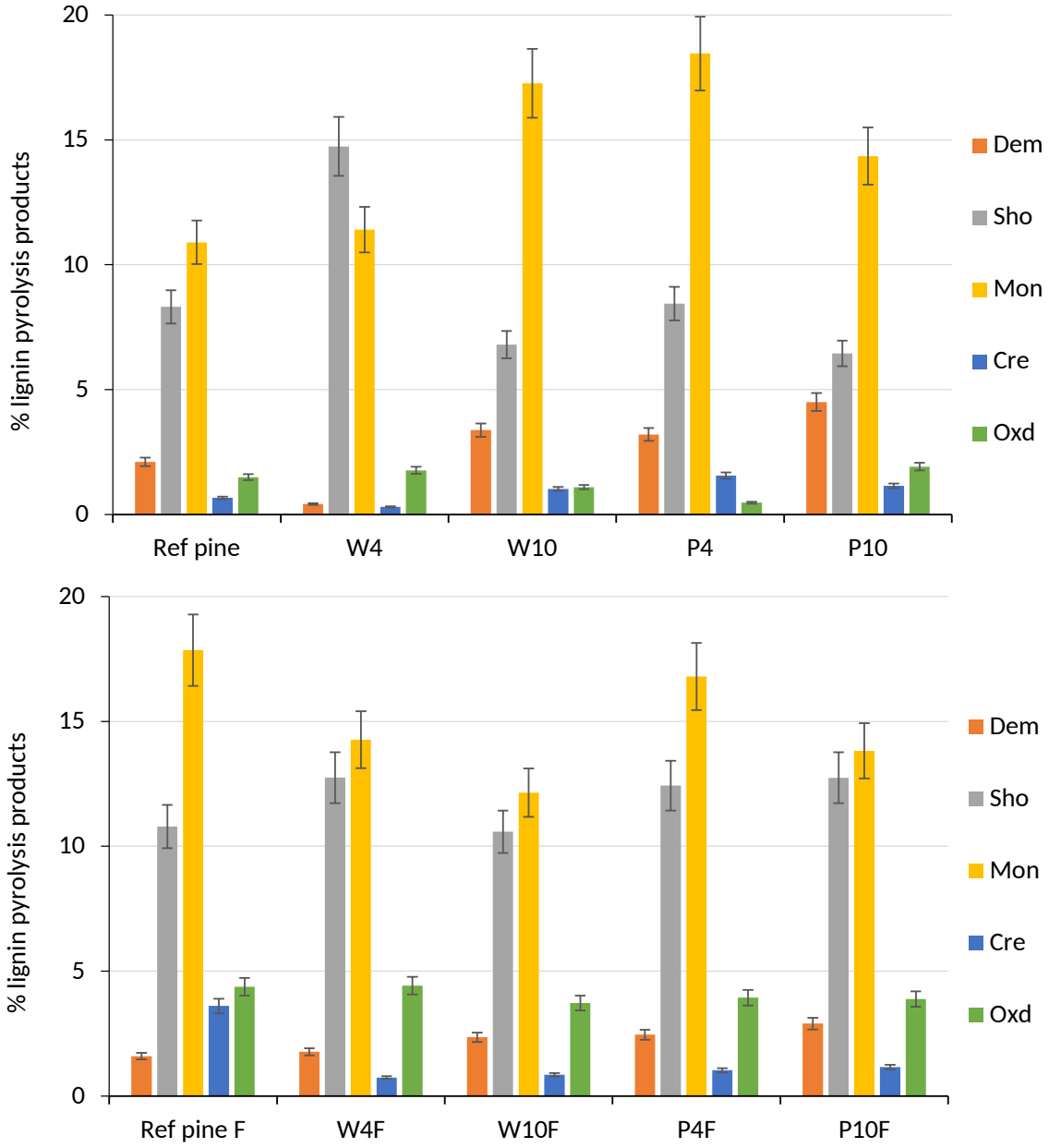

Figure 11. Distribution of categories of lignin pyrolysis products expressed as percentages for the samples before **(a)** and after **(b)** fungal attack.

3.5 XRD

All the samples were analysed by XRD, in order to investigate changes in cellulose crystallinity. Table 3 reports the obtained crystallinity indexes. The results showed that the crystallinity index in the reference pine sample was 0.35. The value slightly increased after four years of burial in both wet peat and lake water (CI = 0.45). This indicated that during the first four years the chemical changes involved mainly the amorphous part of cellulose, whereas the crystalline part remained unaltered. After ten years of burial, the CI values decreased, reaching 0.43 and 0.41 for wet peat and lake water respectively, thus

indicating that at this stage also the crystalline regions began to undergo chemical changes.

The action of fungi caused a significant increase in the crystallinity index of all the samples analysed. These data suggested that in the adopted conditions the fungi preferentially attack the amorphous part of cellulose. According to the literature [26, 60], amorphous cellulose is more susceptible than crystalline cellulose to hydrolysis reactions, since it is more accessible to water and microorganisms.

Table 3. Crystallinity indexes determined by XRD analysis of the pine wood samples before and after *C. puteana* attack obtained using the Segal method [47]

Before fungal attack				
Ref pine	**W4**	**W10**	**P4**	**P10**
0.35	0.45	0.41	0.45	0.43
After fungal attack				
Ref pine F	**W4F**	**W10F**	**P4F**	**P10F**
0.60	0.61	0.60	0.59	0.60

4. Discussion

To extract more information from the analytical data, Py-GC-MS and FTIR data related to the holocellulose and lignin composition were evaluated as follows: the Pearson correlation indexes were calculated to consider the relative amounts of holocellulose categories of pyrolysis products and the ratios between the intensities of IR bands for all the analysed samples.

The examination of the correlation matrix, reported as Supplementary Information S1, highlighted a significant negative correlation between the abundance of furans and those FTIR parameters representing the ratios between the absorption intensity of lignin (band 1508 cm^{-1}) and the absorption intensities of polysaccharides (bands 1730, 1370, 1155 cm^{-1}). This showed clearly that the degradation of carbohydrates induced by fungi is translated during pyrolysis in the production of a relatively higher abundance of furans. The increase in the production of furans during the pyrolysis of wood exposed to fungi is accompanied by a decrease in the intensity of low molecular weight pyrolysis products of holocellulose. Therefore, both the increase of furans and the decrease of low molecular weight pyrolysis products of holocellulose can be considered as chemical markers of the action of this type of brown rot fungi.

There is also evident correlation between the relative abundances of furans and oxidised products of lignin, which both tend to increase during fungal attack, showing how the exposure to fungi has induced an oxidation of the lignin component.

An overall interpretation of the obtained data enabled the following analytical parameters to be highlighted, which can be related to the action of fungi:

- the pyrolysis parameter Smo/Fur representing the ratio between the abundance of low molecular weight pyrolysis products of holocellulose and furans;
- the FTIR parameter 1730/897, representing the ratio between the intensities of the band at 1730 cm^{-1}, associated to hemicelluloses, and the intensity of the band at 897 cm^{-1}, associated to cellulose.

The values of these two parameters are reported in Figure 12 as a scatter plot of all the analysed wood samples. The samples subjected to fungal action appear separated in the scatter plot from the samples which have only undergone burial degradation. In fact, the action of fungi induced an increase in the relative intensity of FTIR signals related to hemicelluloses, and a relative increase in furans in the pyrolytic profile.
Information reported in the literature does not allow us to distinguish the pyrolysis products of cellulose and hemicelluloses, or of crystalline and amorphous cellulose. Thus, it is not straightforward to interpret the variation in the pyrolytic profiles and associate it to a specific chemical change. Nevertheless, there is a clear trend in the analytical parameters considered, which differentiates the fungal-degraded polysaccharides from the polysaccharides which have only undergone burial degradation. XRD provided complementary information by highlighting that the amorphous component of cellulose was mainly targeted by the fungi.

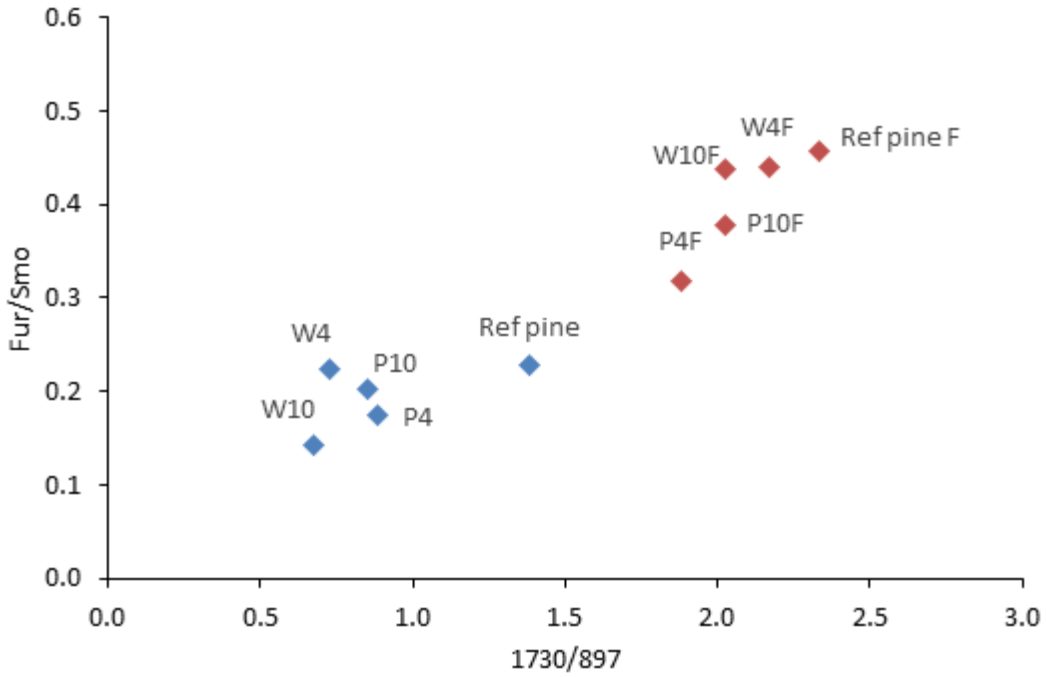

Figure 12. Scatter plot of the values of the pyrolysis parameter Smo/Fur (ratio between the abundance of low molecular weight pyrolysis products of holocellulose and furans) and the FTIR parameter 1730/897 (ratio between the intensities of the band at 1730 cm^{-1}, associated to hemicelluloses, and the intensity of the band at 897 cm^{-1}, associated to cellulose) for all the analysed wood samples.

5. Conclusions

Measurements of mass loss were combined with SEM, FTIR, Py(HMDS)-GC-MS and XRD analysis, thereby permitting an evaluation of some physical and chemical changes induced by ageing in natural environments and by exposure to brown rot fungus *C. puteana* on pine wood samples.

SEM enabled the most degraded samples to be characterised in terms of structural and morphological alterations. FTIR measurements were confirmed to be a valuable tool to establish the state of preservation of wood on the basis of specific ratios calculated between selected FTIR peak intensities. The degradation of holocellulose was observed by FTIR after shorter time of burial in lake water than in peat, suggesting that a reburial of archaeological wood in peat could be favoured over water in terms of preservation of carbohydrates. In addition, FTIR spectra highlighted that the burial in wet environments, peat and lake water, had a different effect compared to the fungal attack on the polysaccharides present in the wood. The wet environments mostly caused changes in the hemicelluloses, whereas the fungal attack was mainly directed towards cellulose degradation.

Data obtained by Py(HMDS)-GC-MS were interpreted by grouping the pyrolysis products into categories according to their chemical and structural features, and evaluating the changes in their relative abundance. The burial in wet environments resulted in an increase in the relative abundance of anhydrosugars, leading to depolymerisation and degradation of polysaccharides. The pyrolysis profiles of the wood samples exposed to the action of *C. puteana* displayed an increase in the relative abundances of furans (Fur) among the pyrolysis products of polysaccharides, accompanied by a decrease in the abundance of small molecular weight pyrolysis products (Smo). The ratio Fur/Smo showed a high positive correlation with the FTIR parameter represented by the ratio between the intensities of the FTIR band at 1730 cm^{-1}, associated with hemicelluloses, and the intensity of the band at 897 cm^{-1}, associated with cellulose. The values of these two parameters increased in fungal-degraded wood, and differentiated the polysaccharides in the samples before and after exposure to fungal attack.

The effect of the action of *C. puteana* on lignin was less evident than on polysaccharides. Nevertheless, in all the samples a certain degree of oxidation of lignin was observed after the action of fungi.

XRD revealed that the crystallinity index of cellulose increased in all analysed samples when compared to reference pine. The increase in the crystallinity index was more evident after fungal attack than after natural ageing in both wet environments, showing that during the exposure to fungi, amorphous cellulose was relatively more degraded than crystalline cellulose.

Acknowledgemnts

The authors would like to acknowledge Prof. Prądzyński and Dr. L. Babiński for support and useful discussions, and Prof. M. Mamonova for contributing to SEM analysis. As an Andrew W. Mellon Postdoctoral Research Fellow, Dr. Diego Tamburini would like to thank the Foundation. The research was carried out within the framework of the Project “Wet archaeological wooden material: a multianalytical approach for decay diagnosis” (2017-2019), Agreement of Scientific Cooperation between the Italian National Research Council of Italy (CNR) and the Polish Academy of Sciences (PAN).

References

[1] L. Babiński, M. Fejfer, W. Prądzyński, Environmental Monitoring at the Lusatian Culture Settlement in Biskupin, Poland, in: B. Coles (Ed.) Journal of Wetland Archaeology Oxbow Books, Oxford, 2007, pp. 51–72.

[2] T. Cesar, T. Danevčič, K. Kavkler, D. Stopar, Melamine polymerization in organic solutions and waterlogged archaeological wood studied by FTIR spectroscopy, Journal of Cultural Heritage, 23 (2017) 106-110.

[3] M. Broda, B. Mazela, Application of methyltrimethoxysilane to increase dimensional stability of waterlogged wood, Journal of Cultural Heritage, 25 (2017) 149-156.

[4] Z. Walsh, E.R. Janeček, J.T. Hodgkinson, J. Sedlmair, A. Koutsioubas, D.R. Spring, M. Welch, C.J. Hirschmugl, C. Toprakcioglu, J.R. Nitschke, M. Jones, O.A. Scherman, Multifunctional supramolecular polymer networks as next-generation consolidants for archaeological wood conservation, Proc. Natl. Acad. Sci. U. S. A., 111 (2014) 17743-17748.

[5] G. Cavallaro, G. Lazzara, S. Milioto, F. Parisi, V. Sparacino, Thermal and dynamic mechanical properties of beeswax-halloysite nanocomposites for consolidating waterlogged archaeological woods, Polym. Degrad. Stab., 120 (2015) 220-225.

[6] G. Cavallaro, G. Lazzara, S. Milioto, F. Parisi, F. Ruisi, Nanocomposites based on esterified colophony and halloysite clay nanotubes as consolidants for waterlogged archaeological woods, Cellulose, 24 (2017) 3367-3376.

[7] J. Kostrzewski, Prasłowiański gród w Biskupinie w pow. żnińskim, Ziemia, 9 (1936) 217-224.

[8] A.P. Singh, A review of microbial decay types found in wooden objects of cultural heritage recovered from buried and waterlogged environments, Journal of Cultural Heritage, 13 (2012) S16–S20.

[9] R.A. Blanchette, A review of microbial deterioration found in archaeological wood from different environments, Int. Biodeterior. Biodegrad., 46 (2000) 189-204.

[10] T. Nilsson, Comparative study of the cellulolytic activity of white-rot and brown-rot fungi, Mater. Org. (Berl.), 9 (1974) 173-198.

[11] T.L. Highley, Cellulolytic Activity of Brown-Rot and White-Rot Fungi on Solid Media, Holzforschung - International Journal of the Biology, Chemistry, Physics and Technology of Wood, 1988, pp. 211.

[12] T.L. Highley, Cellulose Degradation by Cellulose-Clearing and Non-Cellulose-Clearing Brown-Rot Fungi, Appl. Environ. Microbiol., 40 (1980) 1145-1147.

[13] T.L. Highley, Hemicellulases of white- and brown-rot fungi in relation to host preferences, Mater. Org., 11 (1976) 33-46.

[14] B.L. Illman, T.L. Highley, Decomposition of Wood by Brown-Rot Fungi, in: C.E. O'Rear, G.C. Llewellyn (Eds.) Biodeterioration Research 2: General Biodeterioration, Degradation, Mycotoxins, Biotoxins, and Wood Decay, Springer US, Boston, MA, 1989, pp. 465-484.

764 [15] D.J. Yelle, J. Ralph, F. Lu, K.E. Hammel, Evidence for cleavage of lignin by a brown rot
765 basidiomycete, Environ. Microbiol., 10 (2008) 1844-1849.
766 [16] A.T. Martínez, J. Rencoret, L. Nieto, J. Jiménez-Barbero, A. Gutiérrez, J.C. del Río, Selective
767 lignin and polysaccharide removal in natural fungal decay of wood as evidenced by in situ
768 structural analyses, Environ. Microbiol., 13 (2011) 96-107.
769 [17] T.R. Filley, G.D. Cody, B. Goodell, J. Jellison, C. Noser, A. Ostrofsky, Lignin demethylation
770 and polysaccharide decomposition in spruce sapwood degraded by brown rot fungi, Org.
771 Geochem., 33 (2002) 111-124.
772 [18] M.M. Mulder, J.B.M. Pureveen, J.J. Boon, A.T. Martinez, An analytical pyrolysis mass
773 spectrometric study of Eucryphia cordifolia wood decayed by white-rot and brown-rot fungi, J. Anal.
774 Appl. Pyrolysis, 19 (1991) 175-191.
775 [19] C. Sanchez, Lignocellulosic residues: Biodegradation and bioconversion by fungi, Biotechnol.
776 Adv., 27 (2009) 185-194.
777 [20] M.C. Terron, M.L. Fidalgo, G.C. Galletti, A.E. Gonzalez, Pyrolysis-gas chromatography/mass
778 spectrometry of milled wood lignin of two Chilean woods naturally decayed by Ganoderma
779 australe, Phlebia chrysocrea and a brown-rot fungus, J. Anal. Appl. Pyrolysis, 33 (1995) 61-75.
780 [21] J.C. del Río, A. Gutiérrez, M.J. Martínez, A.T. Martínez, Py-GC/MS study of *eucalyptus*
781 *globulus* wood treated with different fungi, J. Anal. Appl. Pyrolysis, 58-59 (2001) 441-452.
782 [22] K.K. Pandey, A.J. Pitman, FTIR studies of the changes in wood chemistry following decay by
783 brown-rot and white-rot fungi, Int. Biodeterior. Biodegrad., 52 (2003) 151-160.
784 [23] E.D. Tomak, E. Topaloglu, E. Gumuskaya, U.C. Yildiz, N. Ay, An FT-IR study of the changes
785 in chemical composition of bamboo degraded by brown-rot fungi, Int. Biodeterior. Biodegrad., 85
786 (2013) 131-138.
787 [24] S. Durmaz, Ö. Özgenç, İ.H. Boyacı, Ü.C. Yıldız, E. Erişir, Examination of the chemical
788 changes in spruce wood degraded by brown-rot fungi using FT-IR and FT-Raman spectroscopy,
789 Vib. Spectrosc., 85 (2016) 202-207.
790 [25] G. Xu, L. Wang, J. Liu, J. Wu, FTIR and XPS analysis of the changes in bamboo chemical
791 structure decayed by white-rot and brown-rot fungi, Appl. Surf. Sci., 280 (2013) 799-805.
792 [26] X. Ge, L. Wang, J. Hou, B. Rong, X. Yue, S. Zhang, The effects of brown-rot decay on select
793 wood properties of poplar (Populus cathayana Rehd.) and its mechanism of action,
794 Holzforschung, 2017, pp. 355.
795 [27] C. Howell, A.C. Steenkjær Hastrup, B. Goodell, J. Jellison, Temporal changes in wood
796 crystalline cellulose during degradation by brown rot fungi, Int. Biodeterior. Biodegrad., 63 (2009)
797 414-419.
798 [28] E. Hocker, G. Almkvist, M. Sahlstedt, The Vasa experience with polyethylene glycol: A
799 conservator's perspective, Journal of Cultural Heritage, 13 (2012) S175-S182.

800 [29] C.M.A. McQueen, D. Tamburini, J.J. Łucejko, S. Braovac, F. Gambineri, F. Modugno, M.P.
801 Colombini, H. Kutzke, New insights into the degradation processes and influence of the
802 conservation treatment in alum-treated wood from the Oseberg collection, Microchem. J., 132
803 (2017) 119-129.
804 [30] F. Bettazzi, G. Giachi, G. Staccioli, S. Chimichi, N. Macchioni, Chemical and physical
805 characterisation of wood of shipwrecks discovered in the ancient harbour of Pisa (Tuscany-Italy) in:
806 P. Hoffmann, J.A. Spriggs, K. Strætkvern, D. Gregory (Eds.) 9th ICOM Group on Wet Organic
807 Archaeological Materials, International Council of Museums (ICOM), Copenhagen 2004, pp. 127-
808 143.
809 [31] M. Riggio, J. Sandak, A. Sandak, D. Pauliny, L. Babiński, Analysis and prediction of selected
810 mechanical/dynamic properties of wood after short and long-term waterlogging, Construction and
811 Building Materials, 68 (2014) 444-454.
812 [32] D. Tamburini, J.J. Łucejko, M. Zborowska, F. Modugno, W. Prądzyński, M.P. Colombini,
813 Archaeological wood degradation at the site of Biskupin (Poland): wet chemical analysis and
814 evaluation of specific Py-GC/MS profiles, J. Anal. Appl. Pyrolysis, 115 (2015) 7-15.
815 [33] B. Waliszewska, M. Zborowska, W. Prądzyński, L. Babiński, J. Kudela, Characterisation of
816 2700-year old wood from Biskupin, Wood Res., 52 (2007) 11-22.
817 [34] M. Zborowska, L. Babiński, B. Waliszewska, W. Prądzyński, Chemical Characterisation of
818 archaeological oak- and pinewood from Biskupin, in: S. Kurjatko, J. Kudela, R. Lagana (Eds.) The
819 5th International Symposium Wood Structure and Properties, Sielnica, Slovakia, 2006, pp. 431-
820 434.
821 [35] D. Tamburini, J.J. Łucejko, M. Zborowska, F. Modugno, E. Cantisani, M. Mamoňová, M.P.
822 Colombini, The short-term degradation of cellulosic pulp in lake water and peat soil: A multi-
823 analytical study from the micro to the molecular level, Int. Biodeterior. Biodegrad., 116 (2017) 243-
824 259.
825 [36] J.J. Łucejko, F. Modugno, E. Ribechini, D. Tamburini, M.P. Colombini, Analytical instrumental
826 techniques to study archaeological wood degradation, Applied Spectroscopy Reviews, 50 (2015)
827 584-625.
828 [37] I. Modzelewska, M. Zborowska, J. Kúdela, L. Babiński, Changes in strenght properties of
829 wood pulp after two years of natural degradation, Wood Res., 57 (2012) 131-142.
830 [38] M. Schwanninger, J.C. Rodrigues, H. Pereira, B. Hinterstoisser, Effects of short-time vibratory
831 ball milling on the shape of FT-IR spectra of wood and cellulose, Vib. Spectrosc., 36 (2004) 23–40.
832 [39] O. Faix Classification of Lignins from Different Botanical Origins by FT-IR Spectroscopy,
833 Holzforschung, 45 (1991) 21-28.
834 [40] J.J. Łucejko, M. Zborowska, F. Modugno, M.P. Colombini, W. Pradzynski, Analytical pyrolysis
835 vs. classical wet chemical analysis to assess the decay of archaeological waterlogged wood, Anal.
836 Chim. Acta, 745 (2012) 70-77.

837 [41] D. Tamburini, J.J. Łucejko, F. Modugno, M.P. Colombini, Combined pyrolysis-based
838 techniques to evaluate the state of preservation of archaeological wood in the presence of
839 consolidating agents, J. Anal. Appl. Pyrolysis, 112 (2016) 429-441.
840 [42] L. Zoia, D. Tamburini, M. Orlandi, J.J. Łucejko, A. Salanti, E.-L. Tolppa, F. Modugno, M.P.
841 Colombini, Chemical characterisation of the whole plant cell wall of archaeological wood: an
842 integrated approach, Anal. Bioanal. Chem., (2017) 1-13.
843 [43] M. Traoré, J. Kaal, A. Martínez Cortizas, Potential of pyrolysis-GC–MS molecular fingerprint as
844 a proxy of Modern Age Iberian shipwreck wood preservation, J. Anal. Appl. Pyrolysis, 126 (2017)
845 1-13.
846 [44] M. Mattonai, D. Tamburini, M.P. Colombini, E. Ribechini, Timing in Analytical Pyrolysis:
847 Py(HMDS)-GC/MS of Glucose and Cellulose Using Online Micro Reaction Sampler, Anal. Chem.,
848 88 (2016) 9318-9325.
849 [45] EN 113 Wood preservatives test method for determining the protective effectiveness against
850 wood destroying basidiomycetes determination of the toxic values, CEN - EN 113, European
851 Committee for Standardization, 1996.
852 [46] D. Tamburini, J.J. Łucejko, E. Ribechini, M.P. Colombini, New markers of natural and
853 anthropogenic chemical alteration of archaeological lignin revealed by in situ pyrolysis/silylation-
854 gas chromatography-mass spectrometry, J. Anal. Appl. Pyrolysis, 118 (2016) 249-258.
855 [47] L. Segal, J.J. Creely, A.E.J. Martin, C.M. Conrad, An empirical method for estimating the
856 degree of crystallinity of native cellulose using the x-ray diffractometer., Text. Res. J., 29 (1959)
857 786-794.
858 [48] A.D. French, Idealized powder diffraction patterns for cellulose polymorphs, Cellulose, 21
859 (2014) 885-896.
860 [49] S. Park, J. Baker, M. Himmel, P. Parilla, D. Johnson, Cellulose crystallinity index:
861 measurement techniques and their impact on interpreting cellulase performance, Biotechnol.
862 Biofuels, 3 (2010) 1-10.
863 [50] Y. Yue, J. Han, G. Han, Q. Zhang, A.D. French, Q. Wu, Characterization of cellulose I/II hybrid
864 fibers isolated from energycane bagasse during the delignification process: Morphology,
865 crystallinity and percentage estimation, Carbohydr. Polym., 133 (2015) 438-447.
866 [51] A.D. French, M. Santiago Cintrón, Cellulose polymorphy, crystallite size, and the Segal
867 Crystallinity Index, Cellulose, 20 (2013) 583-588.
868 [52] G. Kleist, U. Schmitt, Characterisation of a Soft Rot-Like Decay Pattern Caused by
869 Coniophora puteana (Schum.) Karst. in Sapelli Wood (Entandrophragma cylindricum Sprague),
870 Holzforschung, 2001, pp. 573.
871 [53] J.I. Hedges, G.L. Cowie, J.R. Ertel, R. James Barbour, P.G. Hatcher, Degradation of
872 carbohydrates and lignins in buried woods, Geochim. Cosmochim. Acta, 49 (1985) 701-711.

873 [54] J.I. Hedges, The Chemistry of Archaeological Wood, in: R.M. Rowell, R.J. Barbour (Eds.)
874 Archaeological Wood, American Chemical Society, Washington, 1990, pp. 111-140.
875 [55] R.M. Rowell, R.J. Barbour, Archaeological Wood Properties, Chemistry, and Preservation,
876 American Chemical Society, Washington, 1990.
877 [56] D. Tamburini, J.J. Łucejko, E. Ribechini, M.P. Colombini, Snapshots of lignin oxidation and
878 depolymerization in archaeological wood: an EGA-MS study, J. Mass Spectrom., 50 (2015) 1103-
879 1113.
880 [57] S.C. Moldoveanu, Analytical Pyrolysis of Polymeric Carbohydrates, in: D. Coleman, B.F. Price
881 (Eds.) Analytical Pyrolysis of Natural Organic Polymers, Elsevier Science, Amsterdam, 1998, pp.
882 217-316.
883 [58] T. Hosoya, H. Kawamoto, S. Saka, Secondary reactions of lignin-derived primary tar
884 components, J. Anal. Appl. Pyrolysis, 83 (2008) 78-87.
885 [59] M. Asmadi, H. Kawamoto, S. Saka, Thermal reactivities of catechols/pyrogallols and
886 cresols/xylenols as lignin pyrolysis intermediates, J. Anal. Appl. Pyrolysis, 92 (2011) 76-87.
887 [60] R.M. Rowell, R. Pettersen, J.S. Han, J.S. Rowell, M.A. Tshabalala, Cell Wall Chemistry, in:
888 R.M. Rowell (Ed.) Handbook of Wood Chemistry and Wood Composites CRC, Boca Raton,
889 London, New York, Singapore, 2005, pp. 37-76.

890

891

Supplementary material

S1. Correlation matrix reporting the Pearson correlation indexes of the relative abundance of the categories of pyrolysis products and of the ratios calculated between the selected FTIR bands intensities. Categories of pyrolysis products of holocellulose: Ahs- anhydrosugars, Cyp- cyclopentenones, Fur-furans, Hyb-hydroxybenzenes, Pyr – pyrans. Categories of pyrolysis products of lignin: Oxd- oxidation products, Dem- demethylation/demethoxylation products, Sho-units with altered 3-carbon side chains and shorter side chains (1- or 2-carbon), Mon-monomers, Cre-cresols, Smo- small molecules with 1 to 3 carbon. H/L: pyrolytic holocellulose versus lignin ratio. Selected FTIR bands: 1730 cm^{-1} stretching of unconjugated C=O in xylans; 1370 cm^{-1} C–H deformation in cellulose and hemicelluloses; 1155 cm^{-1} C–O–C vibration in cellulose and hemicelluloses; 897 cm^{-1} C–H deformation in cellulose.

	Ahs	Cyp	Fur	Hyb	Pyr	Oxd	Dem	Sho	Mon	Cre	Smo	H/L	1508/1730	1508/1370	1508/1155	1508/897
Ahs	1.00															
Cyp	-0.19	1.00														
Fur	-0.53	-0.35	1.00													
Hyb	-0.61	-0.13	0.53	1.00												
Pyr	0.25	-0.26	0.24	-0.55	1.00											
Oxd	-0.38	-0.34	0.89	0.64	0.02	1.00										
Dem	0.59	0.06	-0.66	-0.01	-0.58	-0.30	1.00									
Sho	-0.52	-0.37	0.75	0.30	0.45	0.59	-0.77	1.00								
Mon	-0.12	-0.44	-0.10	0.34	-0.62	-0.03	0.36	-0.28	1.00							
Cre	-0.39	-0.08	0.28	0.51	-0.47	0.29	0.05	-0.16	0.62	1.00						
Smo	-0.22	0.13	-0.38	-0.41	0.20	-0.66	-0.33	0.03	0.03	-0.33	1.00					
H/L	0.45	0.68	-0.47	-0.57	0.26	-0.51	0.14	-0.48	-0.68	-0.47	0.10	1.00				
1508/1730	0.33	0.33	-0.87	-0.63	-0.15	-0.78	0.42	-0.50	0.08	-0.32	0.51	0.28	1.00			
1508/1370	0.32	0.63	-0.92	-0.47	-0.32	-0.88	0.49	-0.70	-0.02	-0.19	0.39	0.58	0.80	1.00		
1508/1155	0.13	0.53	-0.82	-0.57	-0.21	-0.86	0.28	-0.62	0.14	-0.04	0.60	0.39	0.87	0.88	1.00	
1508/897	0.14	-0.41	0.56	0.47	0.00	0.82	0.17	0.26	-0.06	0.14	-0.88	-0.30	-0.61	-0.68	-0.83	1.00